Universidad Técnica Federico Santa María

Department of Electronics

Valparaíso, Chile

UNIVERSIDAD TECNICA
FEDERICO SANTA MARIA

Modeling and Control of Electrodialysis Process.

Pablo Esteban Yáñez Riquelme

Degree thesis submitted as a partial requirement for the title of
Master of Science in Electronic Engineering.

Thesis Director: Dr. Héctor Ramírez Estay

CONSTANCIA DE VALIDACIÓN Y CONFIDENCIALIDAD DE MONOGRAFÍA A REPOSITORIO ACADÉMICO

1.- IDENTIFICACIÓN DEL TRABAJO ACADÉMICO

Tipo de monografía (marcar una opción): ☐ Memoria o trabajo de título X Tesis de Postgrado

Título del trabajo: Modeling and Control of Electrodialysis Process.

Nombre del candidato(a): Pablo Esteban Yáñez Riquelme.

Carrera / Grado: Magister en Ciencias de la Ingeniería Electrónica – Control Automático

Campus: Casa Central **Departamento:** Electrónica

2.- VALIDACIÓN DEL PROFESOR GUÍA/DIRECTOR DE TESIS

Yo, Héctor Ramírez Estay, en mi calidad de profesor guía del trabajo académico mencionado anteriormente **DEJO CONSTANCIA** que:

- He revisado esta versión del documento y corresponde a la versión final aprobada del trabajo.
- El trabajo cumple con los requisitos académicos y de formato establecidos por la institución.

3.- EVALUACIÓN DE CONFIDENCIALIDAD POR PROPIEDAD INDUSTRIAL (marcar una opción)

X El trabajo **NO contiene** información que amerite confidencialidad y puede ser publicado de inmediato en repositorio con acceso abierto.

☐ El trabajo **CONTIENE** información con potenciales implicancias de propiedad industrial o intelectual y requiere un periodo de confidencialidad (**embargo**) por **(marcar una opción)**:

☐ 6 meses ☐ 12 meses ☐ 2 años ☐ 3 años ☐ 5 años ☐ 10 años

Fundamentación de la necesidad de confidencialidad (obligatorio si se solicita embargo):

N.A.

4.- FIRMAS
Profesor guía de tesis:

Fecha: 09/03/2026 **Firma:** 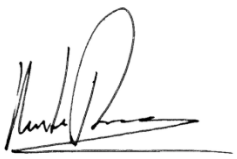

Estudiante:

Fecha: 09/03/2026 **Firma:** 

Dedicado a mis padres: Lady y Patricio

Acknowledgements

Al finalizar esta etapa tan significativa en mi vida, quiero expresar mi más sincero y profundo agradecimiento a quienes me acompañaron y apoyaron durante todo el proceso de mi magíster. En primer lugar, a mi mamá, Lady, y a mi papá, Patricio, quienes han sido un pilar fundamental en mi vida. Su amor incondicional, su apoyo constante y sus palabras de aliento me dieron la fortaleza para superar los desafíos y avanzar con determinación. Sin ustedes, este logro no habría sido posible, y les agradezco desde el fondo de mi corazón por estar siempre a mi lado, creyendo en mí incluso en los momentos más difíciles.

Asimismo, quiero extender mi gratitud al profesor Héctor Ramírez, quien me guió durante el desarrollo de mi tesis. Su conocimiento, compromiso y por sobre todo paciencia fueron clave para que pudiera llevar a cabo este proyecto con éxito. No solo me brindó herramientas académicas esenciales, sino también una guía humana y profesional que me permitió crecer y superar mis propios límites. Su dedicación y confianza en mi trabajo fueron una inspiración constante, y le estoy profundamente agradecido por todo el tiempo y esfuerzo que invirtió en mi formación… que fue extensa.

Este logro es también de ustedes, quienes me apoyaron, guiaron y creyeron en mí desde el principio. A todos, gracias por ser parte de este sueño y por ayudarme a convertirlo en una realidad. Estoy eternamente agradecido por todo lo que han hecho por mí.

Contents

Abstract

This study was developed and validated through industry-applied R&D in an industrial pilot plant at Arauco-Bioforest, in collaboration with AC3E, under ANID Crea y Valida funding program and FONDECYT REGULAR 1231896.

This study aims to find an equivalent electrical model of a laboratory-scale electrodialysis process under pulsed voltage operation (pEDR), considering the number of ion exchange membranes in the process. Subsequently, a practical method is developed to obtain the resistance and capacitance parameters that represent it, along with a calibration method. The equivalent electrical model also incorporates the presence of fouling in the ion exchange membranes in the process, represented again by a resistance and a capacitance.

Once the model is obtained, a controller is generated to minimize fouling in the ion exchange membranes by varying only the duty cycle of the pulsed voltage pEDR method (at a fixed frequency and magnitude of voltage). This is tested in a simulated environment using Simulink MATLAB. The controller employed is the Extremum Seeking Control (ESC) in cascade connection with a PI. In this way, the PI controls the average electrical current (by varying the duty cycle of the pulsed voltage pEDR) of the electrodialysis process, and then the ESC, by measuring the fouling level of the membranes, provides the PI with a new reference for average electrical current to continuously minimize fouling growth during the process operation.

Finally, the controller is tested in a real electrodialysis pilot plant achieving favorable results in the reduction of fouling.

Chapter 1

Introduction

This study was developed and validated in an industrial pilot plant of Arauco-Bioforest, in collaboration with AC3E, as part of R&D activities under ANID Crea y Valida funding program and FONDECYT REGULAR 1231896.

Modeling is a tool that has been used for decades for explaining phenomena and optimizing processes. In the realm of fundamental studies, mathematical models are employed to explain physicochemical phenomena. Conversely, engineering models, which are predicated on operational data, aim to predict the behavior of various processes [10].

Electromembrane technologies, including Electrodialysis (ED), Bipolar Membrane Electrodialysis, Electrodeionization, Selectodialysis, Electrodialysis Reversal, Metathesis ED, Reverse Electrodialysis, Capacitive Deionization, Electro-Electrodialysis, Shock Electrodialysis, Electrodialytic Crystallization, Fuel cells, PEM and AEM electrolysis for hydrogen production, among others, play an important role in various industrial applications due to their efficiency in manipulating ionic components in aqueous solutions. ED, a particularly versatile technique, is probably the most common one, which primarily facilitates the removal of ions from solutions [2]. It can be adapted for a range of applications depending on the configuration of membranes, electrodes, feed order, and fillers. Such adaptations make ED suitable for the recovery of chemicals, energy generation, and the production of ultrapure water, thereby serving diverse industries.

The ED system consists of multiple components such as water pumps, sensors, pipes, power sources, and membrane stacks, each containing a series of cells formed by ion exchange membranes and spacers. These cells are organized in a configuration that positions hundreds between electrodes, an anode and cathode. Unlike filtration methods, ED operates by having the solution flow tangentially across the membranes, separating ions through migration driven by an electric field, established by a potential difference applied in the end electrodes via a direct current. Moreover, the versatility of the ED infrastructure supports alternative operations like Reverse Electrodialysis (RED) [12] [13] [14], which use the same structural components but different operating principles.

Several studies have modeled the ED process, highlighting some aspects such as different electrical models of ED stacks that focus on specific electrochemical behaviors of their layers [3], optimal calculations for limit current densities [24] [5], and energy efficiency [6]. Some researchers also examine the influence of input

effluent composition [7] [8], conducts experiments for parameter identification [9], and investigates systems using only a single ion exchange membrane [10] [11]. The mathematical modeling of electromembrane stacks is notably challenging due to the multitude of factors influencing their performance. Each of these elements can significantly alter the behavior and efficiency of the process, necessitating detailed and multifaceted modeling approaches to capture the nuances of electromembrane operations effectively. These factors include mainly hydrodynamics, electrochemical potential, applied electric field strength, utilization of turbulence promoters, characteristics of ion exchange membranes, temperature, pH, stack geometry, and fouling, biofouling, and scaling of membranes.

Fouling is a common challenge in all types of electromembrane operations, affected by factors like organic foulants nature and concentration [15] [16] [17], and mitigated with reverse polarity operation [19], utilization of anionic surfactants [20], and surface modifications of anion-selective membranes [21]. Fouling often leads to increased energy consumption and maintenance requirements. However, innovative solutions such as pulsed Electrodialysis Reversal (pEDR) or Pulsed Electric Fields (PEF) [22] [23] [24] are employed to mitigate fouling effects, enhancing the system's overall efficiency and lifespan of the membranes, the most expensive components of the stacks. However, studies focusing on pulsed operation of the entire electromembrane stack are limited, as most research primarily examines the effects of pulsed operation on a single membrane rather than the complete stack.

In this study, we developed a hybrid model of electromembrane stacks. This work specifically expands upon the equivalent electrical model of a single ion exchange membrane (IEM) [10]. It hypothesizes that by serially connecting this equivalent electrical system N times, where N represents the number of pairs of ion exchange membranes, a more accurate and realistic model can be achieved by accounting for a variable quantity of IEMs with different properties. The model was expanded to cover fouling of membranes by using a comparison with the electrical resistance growth of an electrodialysis system, based on laboratory experiments. Given the distinctive characteristics of electrodialysis, it was selected as the preferred technique for validating these newly constructed models. This ensures a simple and practical approach for simulation of electromembrane processes.

Automatic control has been used to handle, command, direct, or regulate the behavior of various processes. The need to have or not have a mathematical model of the process to which a controller is desired generally depends on how difficult it is to measure or predict the behavior of that process. There are various control applications in electrodialysis, ranging from energy recovery [25] to improving desalination performance [26]. This work focuses on reducing fouling in membranes, for which Extremum Seeking Control is applied. This controller allows finding a global maximum or minimum of a mathematical model without necessarily having that model [27].

The point of least fouling growth in the ion exchange membranes in the Electrodialyzer occurs at an unknown frequency and duty cycle in the voltage applied to its terminals [22]. Considering what is known about the benefits of this new way of applying pulsed Electrodialysis Reversal (pEDR) [28], higher frequencies and duty cycles above 90% in the applied voltage involve improvements in reducing fouling.

This work also demonstrates how, using a previously obtained equivalent electrical model, in particular the waveform describing the fouling growth of an electrodialysis process, a controller is generated that includes a cascade connection of a PI controller [29] with an Extremum Seeking Control [27]. The operating voltage frequency is fixed, and the duty cycle is adjusted to achieve the least possible fouling growth. The real-time change in the average electrical resistance of the system during operation is observed.

Currently, in the national pulp industry (ARAUCO), AC3E in collaboration with ARAUCO is evaluating these results so that, in the event of a significant reduction in fouling of ion exchange membranes within the electrodialysis process, this solution can be applied to industrial settings. An electrical solution is being developed, capable of switching voltage at adjustable duty cycles and frequencies of up to 8 kHz and powering industrial electrodialyzers with up to 10 kW. The reduced fouling of membranes implies a considerable cost reduction in maintenance, which sparks interest in translating this research into practical applications in the

national industry.

This project is currently funded by CORFO under its "Crea y Valida" program and FONDECYT REGULAR 1231896.

1.1 Organization

This thesis is divided into five main chapters.

- ***Chapter 2:*** Electrical equivalent model of an electromembrane stack and fouling under pulsed operation.
- ***Chapter 3:*** Simulation and results of Extremum seeking control and PI in cascade connection applied to a circuital approximation of an Electrodialysis process.
- ***Chapter 4:*** Results of Extremum seeking control and PI in cascade connection applied to a pilot plant of electrodialysis.
- ***Chapter 5:*** Conclusions and comments on future work are given in this chapter.

1.2 Main Contributions

The main contributions of this thesis can be summarized in the following points:

- This study was an industry-applied research effort, developed and validated in an industrial pilot plant at Arauco-Bioforest, in collaboration with AC3E, as part of R&D activities under ANID's Crea y Valida funding program and FONDECYT REGULAR 1231896.
- An equivalent electrical model of a laboratory-scale electrodialysis process under pulsed voltage operation, considering fouling in its membranes and the number of membranes it comprises. Additionally, a parameter calibration method.
- Implementation of an Extremum Seeking Control (ESC) in cascade with a PI controller to mitigate fouling in the electrodialyzer membranes, varying the duty cycle in the feed voltage of the electrodialyzer.
- Testing in a pilot electrodialysis plant to validate the simulated results of the equivalent electrical model of the plant and the applied control to reduce fouling growth on its membranes.

Chapter 2

Electrical equivalent model

Modeling is essential for understanding phenomena and optimizing processes. Electromembrane technologies like Electrodialysis (ED) are widely used in industries for ion removal, chemical recovery, and ultrapure water production. ED systems rely on electric fields to separate ions, with adaptable configurations for diverse applications.

Fouling, a common issue, increases costs but can be mitigated with methods like reverse polarity and pulsed electric fields, enhancing efficiency and membrane lifespan. This study developed a hybrid model for electromembrane stacks by extending a single-membrane electrical model to account for multiple membranes and fouling, validated through electrodialysis experiments.

Regarding Figure 1, the DC power source, an Asymmetric Bipolar Switch (ABS), and the electrodialyzer (ED) can be observed. The ABS is responsible for taking the DC voltage and switching it to a desired frequency and duty cycle. Therefore, what is modeled in this chapter is the ED under the influence of the switched voltage supplied by the ABS.

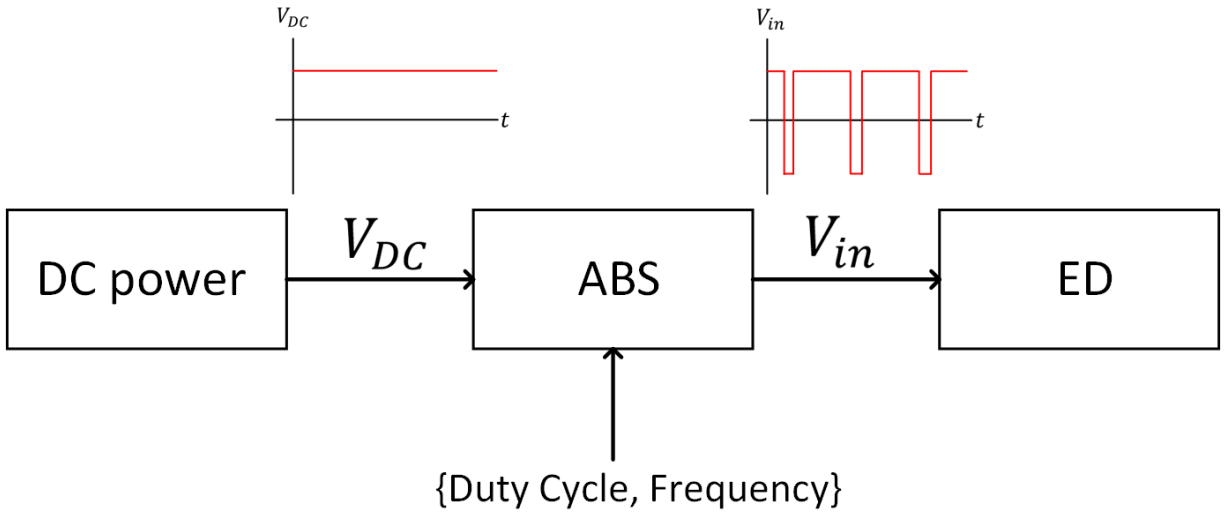

Figure 1: Electrodialysis setup: Connection between ABS, ED, and DC power source.

2.1 Materials and Methods

A proposed equivalent electrical model was designed for electromembrane stacks. A cell structure (a repetitive unit in the stack) was stratified into several layers, which include a bulk solution, diffusion layer, Stern layer, and ion exchange membranes (Figure 2). This model accounts for various components such as membrane resistance (R_M), geometric capacitance (C_M), diffusion layer resistance (R_s), and geometric capacitances (C_{gs} and C_{dl}). To extend the approach to more complex setups, the model has been adapted to include multiple ion exchange membranes. In (2.1) detailing the equivalent impedance of an electromembrane stack with N membranes is provided to support this extension. Additionally, the model addresses fouling by integrating components like fouling resistance (R_f) and capacitance (C_f), whose values are empirically determined. Further details are provided on the chemicals and membranes utilized in the study, along with comprehensive descriptions of the desalination process under pulsed conditions, which previously demonstrated a reduction in the occurrence of fouling.

2.1.1 Basal components of the model

The electromembrane stack is composed of multiple layers, each characterized by distinct electrical properties. Central to this configuration is the ion exchange membrane, characterized by its resistance (R_M), which is influenced by the chemical properties and thickness [12]. For the purposes of this study, it is assumed that the IEM is fully covered by the fluid being treated throughout its entire effective area.

The cell, the basic and repetitive electromembrane unit, typically consists of both anion and cation exchange membranes in ED (Figure 2). This cell is stratified into several distinct layers as mentioned before: a bulk solution (BS), a diffusion layer (DL), a Stern layer (SL), and the IEM. It is important to note that the electric double layer (EDL) comprises both the DL and SL. The distribution of these layers has a specific order, and its extension depends on how many membranesthe electromembrane stack has from electrode to electrode, based on the required flow to be treated.

Within the IEM layer, the geometric capacitance (C_M) is connected in parallel to R_M but is effectively considered negligible (zero farads) because the charge within the IEM layer remains fixed, thus C_M does not

significantly affect the overall model beyond the contribution of $R_{M.}$ The diffusion layer forms as ions migrate through the membranes from the bulk solution, under an electric field. This layer is limited at higher current densities, where no further ions are available on the surface of the membranes, known as the Stern layer. Typically, the diffusion layer has a thickness in the order of micrometers. The combined resistance of the diffusion and Stern layers is referred as R_S, and their geometric capacitance, represented as C_{gs} [10], accounts for the charge differences and the width of the double layer, also in the order of micrometers.

Additionally, the diffusion layer, depleted of ions, forms an electrical double layer with the bulk solution, which is rich in fresh ions. This double layer is modeled using the geometric capacitance C_{dl}, considering the charge differences and the width of the Stern layer. Complementary, the Warburg Impedance of finite length, represented by Z_{wo}, is used to model the interaction between layers, and assumes a Donnan equilibrium, reflecting the influence of both the Stern and diffusion layers [10] [30]. Moreover, given the frequency range used in this study ($j\omega \longrightarrow 0$), the effect of Z_{wo} is assumed to be purely resistive.

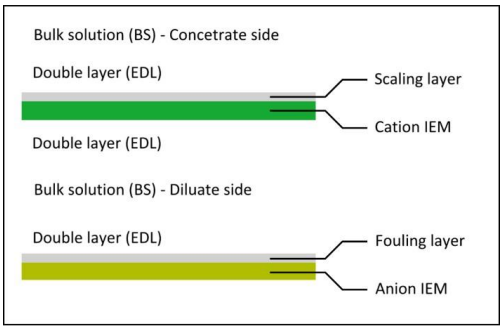

Figure 2: Layers in the electromembrane cell unit that composes a stack, this includes: bulk solution, electric double layer and ion-exchange membranes. It also shows fouling and scaling layer that can accumulate on the surface of ions exchange membranes.

2.1.1.1 Addition of an indefinite number of membranes to the equivalent electrical system

Electronically, each layer within the electromembrane stack is composed of a resistance in parallel with a capacitance, connected in series to the corresponding components of adjacent layers, except for the membrane resistance, which lacks a parallel capacitance. The characteristics of these components are specific to the layer in which they are located.

For configurations involving N ion exchange membranes, the electrical model was derived by integrating models referenced in previous studies [10], with the considerations outlined above and arranging them in series (Figure 3A). This arrangement assumes that all membranes possess uniform properties. Should any membrane, or a group thereof, exhibit distinct physical or chemical properties, it would result in varied electrical behaviors and necessitate additional components in the model.

The multiplicative factor of N is applied by connecting all the membrane subcircuits in series (Figure 3B). By reducing the number of components and obtaining the equivalent circuit, the N factor is multiplied to the resistances and divided by the capacitances, according to (2.1).

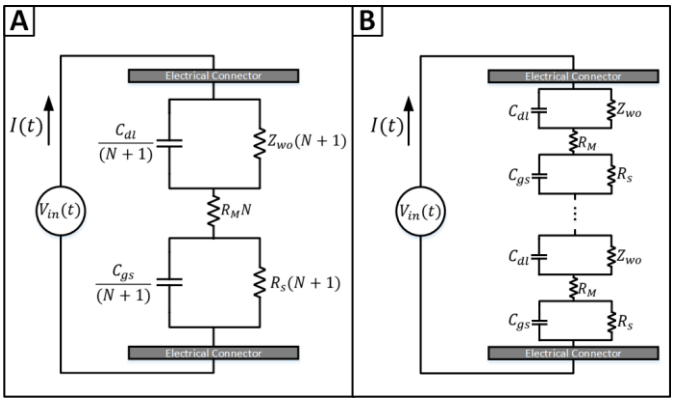

Figure 3: $Z_{StackNoFouling}$: Basal construction of the electromembrane stack model using an electronic approach. A) Equivalent electrical circuit model of the stack. B) Generalization of the equivalent model when integrating different membranes in series.

The equivalent impedance of the electromembrane stack with N membranes is denoted as Z_{Stack}. An "N+1" factor is employed because each additional membrane introduces two identical circuits on both the left and right sides of an ion exchange membrane [10]. However, for R_M specifically, it is multiplied only by N, as it directly correlates to the number of membranes. $Z_{StackNoFouling}$ represents the impedance of the stack without the components that account for fouling (Figure 3), while Z_{Stack}, which includes all components, is shown in Figure 4.

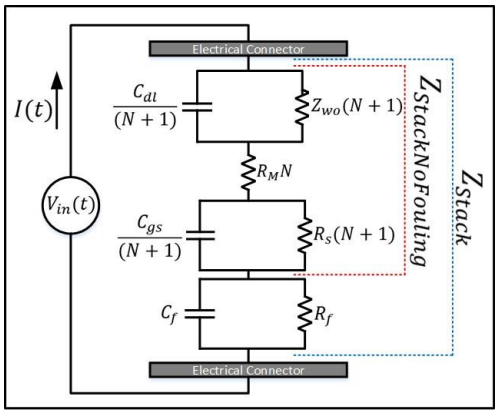

Figure 4: Z_{Stack}: Representation of an equivalent electrical circuit model of an electromembrane stack, with the fouling layer incorporated into the overall model. The model is structured to simulate the electrical behavior of the stack under different operational conditions, including the presence of fouling, which is a common issue in longterm membrane operations

$$Z_{Stack} = \left(\frac{1}{R_s(N+1)} + \frac{C_{gs}}{(N+1)}s\right)^{-1} + \left(\frac{1}{Z_{wo}(N+1)} + \frac{C_{dl}}{(N+1)}s\right)^{-1} + \left(\frac{1}{R_f} + C_f s\right)^{-1} + R_M N \quad (2.1)$$

$$Z_{StackNoFouling} = \left(\frac{1}{R_s(N+1)} + \frac{C_{gs}}{(N+1)}s\right)^{-1} + \left(\frac{1}{Z_{wo}(N+1)} + \frac{C_{dl}}{(N+1)}s\right)^{-1} + R_M N \quad (2.2)$$

2.1.1.2 Incorporation of fouling electric-equivalent components

Fouling and scaling in electromembrane systems occur primarily due to the presence of organics (fouling) and inorganics(scaling), leading to periodic deposition and formation of layers on the membrane surfaces (Figure 2). These layers exhibit resistive and capacitive behaviors. To model them, fouling and scaling are considered equivalent and collectively referred as "fouling"from this point onward, as their impact on voltage and electric current within the electromembrane stack is similar [31].

Fouling is simplified as a layer characterized by a resistance,R_f, and a capacitance, C_f, connected in parallel, similar to other described layers. The values of R_f and C_f primarily depend on the feeding time of the water sample containing foulants. As the electromembrane system runs, fouling increases over time, and the rates at which R_f and C_f change as well when varying the electric current. As mentioned in the introduction, pEDR or PEF operationmodes could decrease the fouling occurrence in electromembrane processes [22].

The values of R_f and C_f are empirically determined based on the fouling observed in an electrodialysis system operating under pEDR or PEF modes with a sample containing foulants. Over a specific period of operation, these components provide an approximation of the growing resistance due to fouling within the system under the given operational conditions.

2.1.2 Chemicals and membranes

NaCl and Na2SO4 (analytical grade) were obtained from Merck Chemicals. Standard desalination membranes PC-SA (anionic exchange) and PC-SK (cationic exchange) were obtained from PCCell GmbH, Germany. PC-SA and PC-SK have an electrical resistance of 1.8 and 2.5 Ωcm^2 respectively.

2.1.3 Electromembrane system

The employed electromembrane system including power supply, pumps, automatic valves, and an electromembrane stack (ED64, PCCell GmbH, Germany). Five pairs of IEMs provided (N=10) a total surface area of $320cm^2$, with an individual membrane area of $64cm^2$. The system was used as electrodialysis for desalting a solution of NaCl, with a linear velocity of 6 L/cm. The electrode compartment had a rising solution of 0.25 M Na2SO4, with a flow rate of 0.4 L/min.

2.1.4 Pulsed operation

Coupling electromembrane stack of an Asymmetric Bipolar Switch (ABS, Anturi SpA, Chile) allows the application of reverse polarity pulses at different conditions, varying frequencies, pulse widths and intensities [28]. In this study, a frequency of 2,000 Hz and 4,000 Hz, an amplitude of 23Vdc, and pulse widths of 10μs and 50μs, were used to validate the model.

2.2 Results and Discussion

The values of the components associated with the electrical equivalent circuit of the electrodialysis process are presented. Subsequently, a method to calibrate these values is introduced, and finally, the components representing fouling are added, thus obtaining the complete and calibrated representation of the electrodialysis system.

2.2.1 Calculation of component values

Initially, the component values associated with the electrical equivalent circuit were computed and analyzed. The accuracy of the equivalent circuit in the electrical model was directly reflected in the electrical current readings. These readings were key to evaluate the effectiveness of the determined values and distribution of components within the modeled circuit. The results obtained from the model provided us insights into the steady-state value of the electric current, the magnitude of electric current peaks, and the settling time required for the transient electric current to reach a steady state when the voltage source is switched during pulsed operation.

Thus, we simulated an ED stack of 5 pairs of ion exchange membranes (N=10) of 64cm^2 of effective area, and 23 Vdc was applied. A voltage drop of 3V was used for the electrodes [28], and the membrane resistance was R_M=107,14Ωcm^2, obtained directly from the peak value of the electric current that divides the continuous supply voltage [12], the capacitance associated with the ion exchange membrane was considered to have a value of zero (given its low charge difference and to facilitate calculations). On the other hand, R_s = 2.6021 Ωcm^2 [10] was obtained assuming that the average electric current is at least 80% of the limiting current density, the temperature of the process was kept constant at 20°C (293.15 °K), with a diffusion coefficient of ions D1 is equal to D2 [10] and effective transport number t1and t2 had a value of 0.5 [10], with an initial concentration of 0.25M NaCl [22] and an empirical value of limiting current density of 15.625 A/cm^2 [22]. Additionally, C_{gs} = 5μF/cm^2 [10] was obtained considering a width of the DBL layer in the order of 100 μm and a relative permittivity of water, in the range of 80 to 100. Z_{wo}= 9.3772 Ωcm^2 [10], was obtained under the same considerations as R_s, but also considering that jω → 0, since the amplitude in its imaginary component was negligible as frequencies in the order of 1MHz were not used, so Z_{wo} was analyzed as a resistor.

Finally, C_{dl} = 43.7 mF/cm^2 [10] was calculated in the EDL layer under the same conditions as above. Then by considering 10 IEMs and a total effective area of 64cm^2, we obtained the final values, shown in Table 1.

Electric Component	Density Value	Total
R_M	107.14Ωcm^2	16.74Ω
C_{dl}	43.7mF/cm^2	254.25mF
C_{gs}	5$\mu F/cm^2$	29.09μF
R_s	2.6021Ωcm^2	0.44723Ω
Z_{wo}	9.3772Ωcm^2	1.6117Ω

Table 1: Values of electric components

The Density Value column represents the resistance or capacitance depending on the effective area of the N=10 IEMs, and the Total column represents the value considering an effective area of 64 cm^2. The values of the components that make up the $Z_{StackNoFouling}$ equation (2.2) is obtained, with this, the electric current can be observed given a constant voltage, pEDR, or PEF signal.

2.2.2 Electric components calibration

When the value of R_M (Figure 5a) changed, only the amplitude of the electric current signal was affected. This is because R_M does not have a parallel capacitance, thus influencing only the magnitude of the current signal. As shown in Figure 5a, even small variations in this component can result in significant changes in the peak and settling value of the electric current reached. Figures 5b and 5c demonstrate that when varying the values of $C_{dl}$and C_{gs}, the settling time of the electric current is primarily impacted.

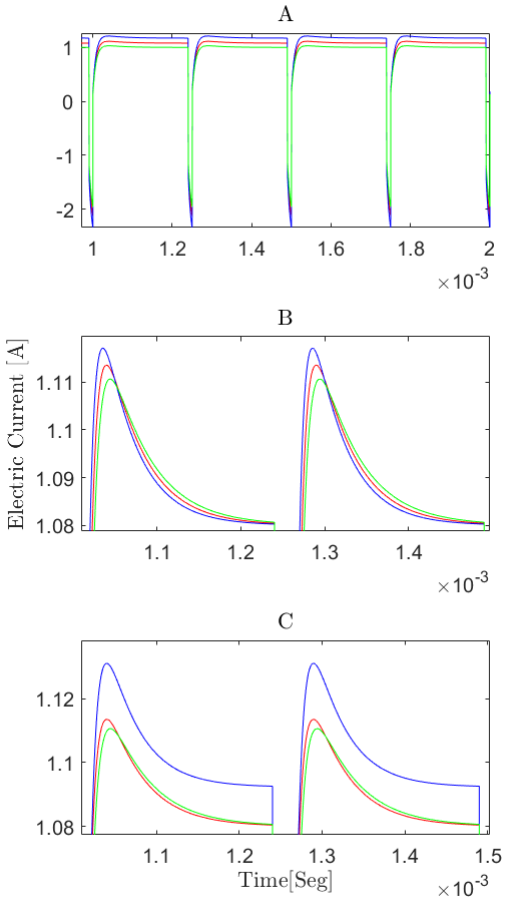

Figure 5: Simulation of T11 experiment [22] with Vin = 23V, 4000 Hz, pulse width of 10 µs: (a) changing R_M ion exchange membrane resistance, with unchanged R_M (red line), 90% of R_M (blue line), and 110% of R_M (green line). (b) changing the capacitances, with C_{dl} and C_{gs} unchanged (red line), C_{dl} and C_{gs} at 90% (blue line), and C_{dl} and C_{gs} at 110% (green line). (c) changing resistances Z_{wo} and R_s, with unchanged (red line), Z_{wo} and R_s at 90% (blue line) and with Z_{wo} and R_s at 110% (green line).

This suggests a straightforward method of calibrating the settling time through adjustments of these components. While Z_{wo} and R_s also undergo changes in magnitude similar to R_M, their total contributions are at least 10 times smaller than the capacitances based on the proportions of the values obtained (as shown in Table 2).

Component	Density Value	Total	Gain
$R_{M-calib.}$	$105.946\Omega cm^2$	16.554Ω	$\alpha_1 = 0.99$
$C_{dl-calib.}$	$43.7mF/cm^2$	$254.254mF$	$\alpha_2 = 1$
$C_{gs-calib.}$	$5\mu F/cm^2$	$29.09\mu F$	$\alpha_3 = 1$
$R_{s-calib.}$	$2.839\Omega cm^2$	0.488Ω	$\alpha_4 = 1.09$
$Z_{wo-calib.}$	$10.223\Omega cm^2$	1.757Ω	$\alpha_5 = 1.09$

Table 2: Values of electric components calibrated

The correction factor α_1 greatly varies the peak and stead-ystate magnitude of the electric current, α_2 together with α_3 only the settling time of the electric current and α_4 together with α_5 the settling time and peak and steady-state magnitude of the electric current but in a small proportion. First, as a calibration method, the laboratory data was obtained from: Peak electrical current value i_{Max} and electrical current value at the instant in which the voltage source switches from positive to negative values (i_{Com}) in pEDR operation. Accordingly, α_1 was varied until the simulated electric current peak value (i_{SimMax}) and the simulated electric current steady-state value (i_{SimCom}) approach to i_{Max} and i_{Com}, respectively, and then α_4 and α_5 were varied for micro tuning purposes of the above. Subsequently, α_2 and α_3 were varied only to adjust the settling time of the electric current in such a way that without a significant change of i_{SimMax}, the value of $i_{SimCom}$was corrected. Finally, if the approximation is not satisfactory (error less than 10%), the process was repeated as shown in the flowchart (Figure 6). The calibration values α must be in the following ranges of (2.8) and (2.9).

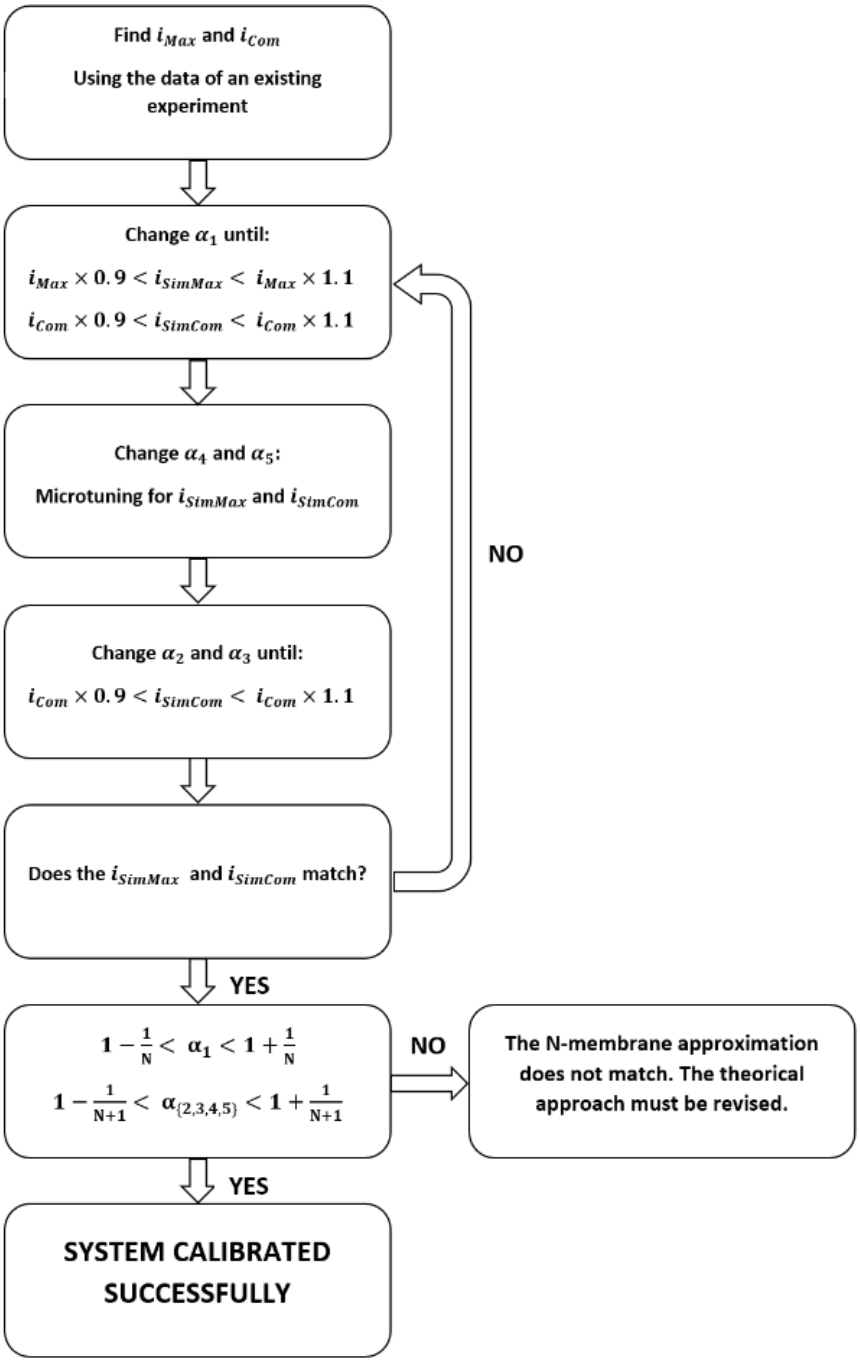

Figure 6: Flowchart of component calibration.

$$R_{M-calib.} = R_M \alpha_1 \tag{2.3}$$

$$C_{dl-calib.} = C_{dl} \alpha_2 \tag{2.4}$$

$$C_{gs-calib.} = C_{gs} \alpha_3 \tag{2.5}$$

$$R_{s-calib.} = R_s \alpha_4 \tag{2.6}$$

$$Z_{wo-calib.} = Z_{wo} \alpha_5 \tag{2.7}$$

$$1 - \frac{1}{N} < \alpha_1 < 1 + \frac{1}{N} \tag{2.8}$$

$$1 - \frac{1}{N+1} < \alpha_{\{2,3,4,5\}} < 1 + \frac{1}{N+1} \tag{2.9}$$

The values of α, as given by (2.8) and (2.9), must be satisfied to ensure an accurate estimation. A no accurate situation could occur when extending the values of the components arithmetically, while considering N ion exchange membranes. In other words, the calibration can deviate by a maximum of 1 IEMs in relation to the total number of IEMs. For example, if $\alpha_1 = 1.21$ with N=10 IEMs, it means that the calibration does not match. In this case, $\alpha_1 = 1.21$ would imply that the electrodialysis system has 12.1 IEMs, which is not consistent with the intended calibration.

2.2.3 Model validation under pulsed operation

In the Equivalent model of the ED obtained (according to Table 3) Applying (2.10), that represents the resistance of ED in steady state, we obtain $Z_{StackNoFouling}(t \to \infty) = 18.7993\ \Omega$ which implies a steady state current of $I(t \to \infty) = 1.06$ A. In order to fully validate the hybrid model, different pEDR operations (Table 4) were simulated with the proposed and calibrated model (Figure 7) and compared with experimental results.

Test	Voltage supply parameters		
	Pulse width [μs]	Frequency [Hz]	pEDR amplitude
T5	50	2,000	0
T6	50	2,000	1
T9	10	4,000	0.2
T11	10	4,000	2

Table 3: The "Pulse width" is the duration in microseconds of the reverse polarity pulse, "pEDR amplitude" is the amplitude of the voltage when it is in the "Pulse width" period.

Test	Electric Current Simulated [A]		Electric Current Empirical [A]	
	i_{SimMax}	i_{SimCom}	i_{Max}	i_{Com}
T5	1.20	1.07	1.13	0.98
T6	1.24	1.17	1.32	1.1
T9	1.19	1.10	1.09	1
T11	1.23	1.17	1.29	1.2

Table 4: Electric current obtained from the simulations and compared with empirical results.

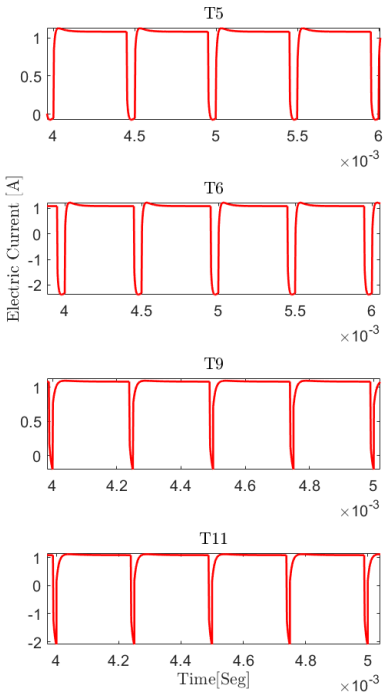

Figure 7: Pulsed operation pEDR simulated. The response in electric current given a voltage of amplitude 23 Volt and frequencies of 2,000 Hz and pulse width of 50µs (T5 and T6) and 4,000 Hz and pulse width of 10µs (T9 and T11).

$$Z_{StackNoFouling}(t \to \infty) = R_s(N+1) + Z_{wo}(N+1) + R_M N \qquad (2.10)$$

The shapes of the electrical current signal obtained in simulation were similar to those obtained in the real experiments [22] (Figure 8). The values of interest are i_{SimMax} and i_{SimCom}, obtaining an error of less than 10% with respect to the empirical results (i_{Max} and i_{Com}), satisfying (2.8) and (2.9).

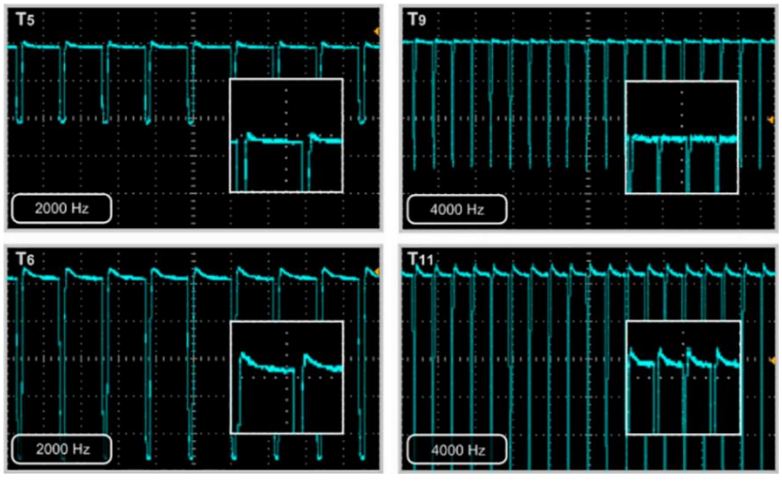

Figure 8: Pulsed operation pEDR over an ED described in section 2.1.4 [22] , The response in electric current given a voltage of amplitude 23 Volt and frequencies of 2,000 Hz(T5 and T6) and 4,000 Hz(T9 and T11).

This study develops a hybrid model for electromembrane stacks, integrating an equivalent electrical circuit and empirical fouling representation to simulate the system's behavior under pulsed operations. By serially connecting ion exchange membranes and incorporating fouling effects, the model achieves high accuracy validated against experimental data, demonstrating less than 10% error. The approach simplifies the representation of electrodialysis systems, enabling practical applications in desalination and other electromembrane technologies while addressing challenges like fouling and scaling through calibrated operational adjustments. This work advances the scalability and reliability of electromembrane-based solutions.

Chapter 3

Control of an electrodialysis process

In this chapter, the simulation includes a voltage switch called Asymmetric Bipolar Switch (ABS) [28], which transforms a constant voltage signal into a voltage signal with a specific frequency, duty cycle (DC_v) and with the same amplitude value of V_{DC} for both the positive and negative voltage switching of V_{in}, connected between the voltage DC power source and the Electrodialyzer (ED). The controller (which acts on the DC_v at a fixed frequency) and the current (I) and voltage (V_{in}) sensors are integrated into the Controller Unit (CU) processor. I is the electrical current entering and exiting the ED, while V_{in} is the voltage applied to its electrical terminals. This setup can be seen in figure 9.

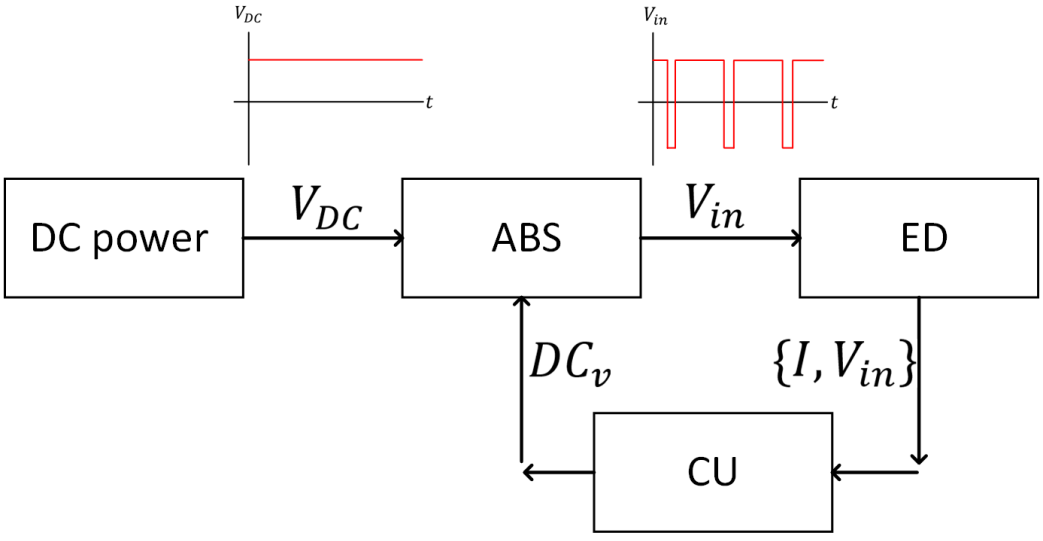

Figure 9: Electrodialysis setup: Connection between ABS, ED, CU, and DC power source.

The application of a controller to the electrodialysis process is examined with a Proportional-Integral Controller (PI). Using a reference electric current I_{ref} to impose a new Duty Cycle DC_v voltage on the ED through PI control facilitates processing calculations. The CU block represents a processing unit (such as a microcontroller) that would not be capable of observing current peaks at high switching frequencies of the input voltage V_{in}, so the average electric current I_{av} is used to simplify computational capacity.

Initially, an analysis of the advantages associated with this control method is conducted. Subsequently, convergence is verified to ensure stability of the close loop PI control. To simulate the controller, it is first necessary to make simplifications to the model presented in Chapter 2 Subsequently.

3.1 Proportional-Integral Control

The electric current $I(t)$ is obtained by applying a voltage pEDR V_{in} to the terminals of the plant. The average of the electric current $I(t)$ is $I_{av}(t)$. $I_{av}(t)$ has a direct proportion, α, with the duty cycle DC_v of the voltage V_{in}. Additionally, since $I_{av}(t)$ is obtained by averaging hundreds of points of $I(t)$, there is a delay, β, in obtaining a new $I_{av}(t)$ given a new value of DC_v.

The equivalent electrical model of the ED together with the ABS (Figure 9) is stable since it is simply a second-order RC network. Because it is stable, it can be reduced to a first-order representation that describes the relation between DC_v and $I_{av}(t)$.

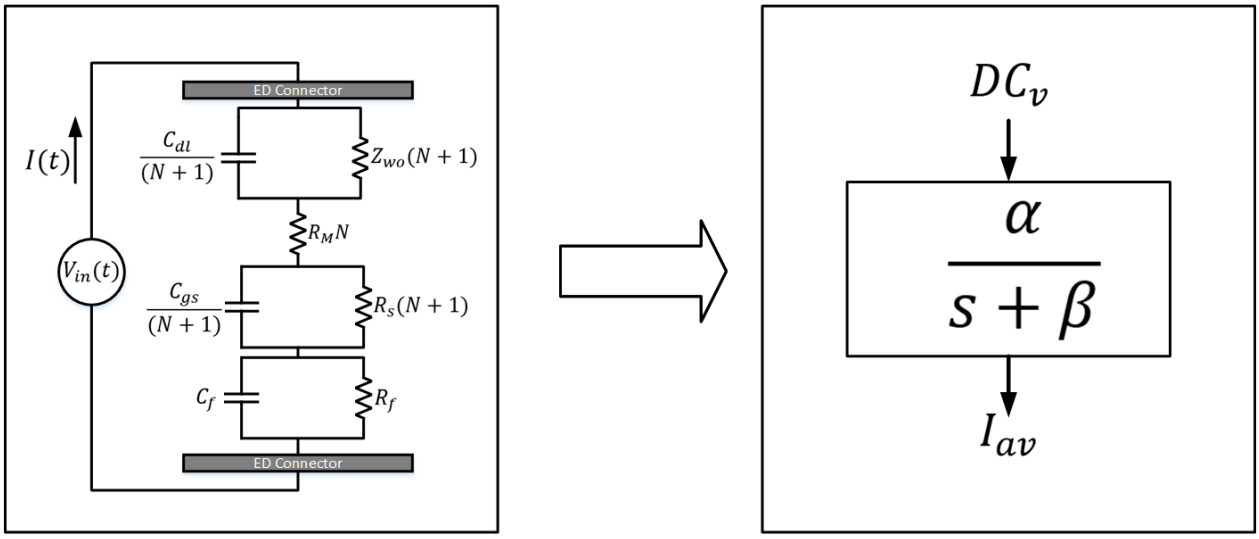

Figure 10: According to [10], Simplified equivalent circuit: Z_{wo} represents the Warburg impedance in the electrical double layer (EDL); C_{dl} represents the electric double layer *capacitance (EDL); R_M represents the resistance of the ion exchange membrane (IEM); R_s represents the resistance of the diffusion boundary layers (DBL); C_{gs} represents the capacitance of the diffusion boundary layers (DBL); and V_{in} represents the voltage supply. Then, according to the simplification, DC_v represents the duty cycle of the voltage V_{in} and I_{av} is the averaged electric current $I(t)$.*

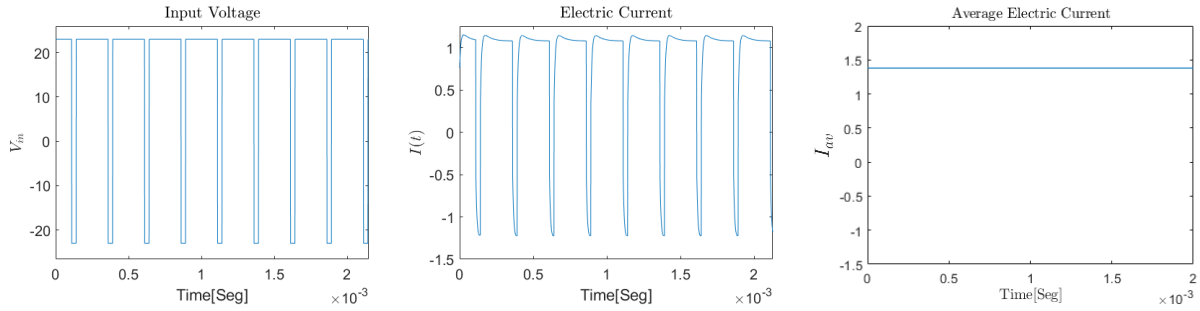

Figure 11: V_{in}: Simulated input voltage $V_{in}(t)$ in the ED with 96% DC_v and 4k hertz. $I(t)$: Simulated electric current $I(t)$ in the ED 96% DC_v and 4k hertz. $I_{av}(t)$: Simulated average electric current $I_{av}(t)$ in the ED 96% DC_v and 4k hertz.

According to figure 13, which illustrates the operation of the PI control, we have the plant ($G(s)$) that includes ABS and ED , that receives the DC_v of the input voltage signal V_{in} (with a fixed frequency) , and the output is electric current and the applied voltage $\{I, V_{in}\}$, which is the average current of the system $I_{av}(t)$ after $I(t)$ has been averaged. $G(s)$ can be simplified as the following transfer function:

$$G(s) = \frac{I_{av}(s)}{DC_v(s)} = \frac{B(s)}{A(s)} = \frac{\alpha}{s+\beta} \tag{3.1}$$

There is a linear relationship between the DC_v and the $I_{av}(t)$, which is represented by the parameter α. And there is a period where the $I_{av}(t)$ stabilizes at αDC_v. This is because when applying a pulsed voltage V_{in}, a pulsed current $I(t)$ is obtained from the system (Figure 11). As the values of the amplitude of the pulsed current $I(t)$ are averaged, the new value of the $I_{av}(t)$ of the system is gradually obtained each time the DC_v value changes, and this is represented by the parameter β.
The values of $\alpha = 0.1$ and the value of $\beta = 0.01$ according to the experiments on [22].

PI Control calculates an error value as the difference between a desired setpoint and a measured process variable and adjusts using proportional and integral terms (k_p and k_i). This allows for accurate and responsive correction in control functions.

In this section, a fundamental theorem on PI Control [29] is used.

Theorem 3.1 *(Nominal internal stability of PI controller) Consider the nominal closed loop depicted in* figure 12 *with the model and the controller defined by the representation given by* $G(s) = \frac{B(s)}{A(s)}$ *and* $C(s) = \frac{P(s)}{L(s)}$ *respectively. Then the nominal closed loop is internally stable if and only if the roots of the nominal closed loop characteristic equation.* $A(s)L(s) + B(s)P(s) = 0$ *all lie in the open left half plane.*

To control the system, the following structure of a PI control ($C(s)$) is proposed:

$$C(s) = \frac{P(s)}{L(s)} = \frac{K_p s + K_I}{s} \tag{3.2}$$

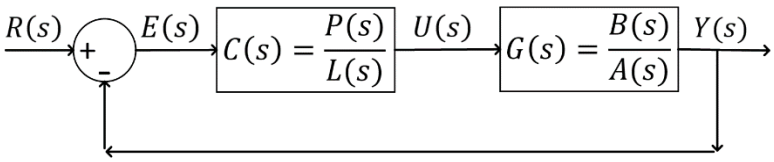

Figure 12: Basic Scheme of PI control C(s) and plant G(s) [29].

$C(s)$ is the PI controller and $G(s)$ is the plant. $E(s)$ is the error between the plant's output $Y(s)$ and the reference $R(s)$ and U(s) is the action applied by the controller to the plant input.

3.1.1 Proposed PI control

Using the structures of figure 9 and figure 12, to ensure that the ED follows a reference average current I_{ref} by acting with DC_v on the voltage V_{in} applied to $G(s)$, the following control scheme is proposed (Figure 13). The processing, which includes the controller C(s) and the acquisition of the average current I_{av} through the MEAN block along with the saturation SAT of the DC_v operating range, is contained within the CU block. On the other hand, the plant G(s) includes both the ABS and the ED.

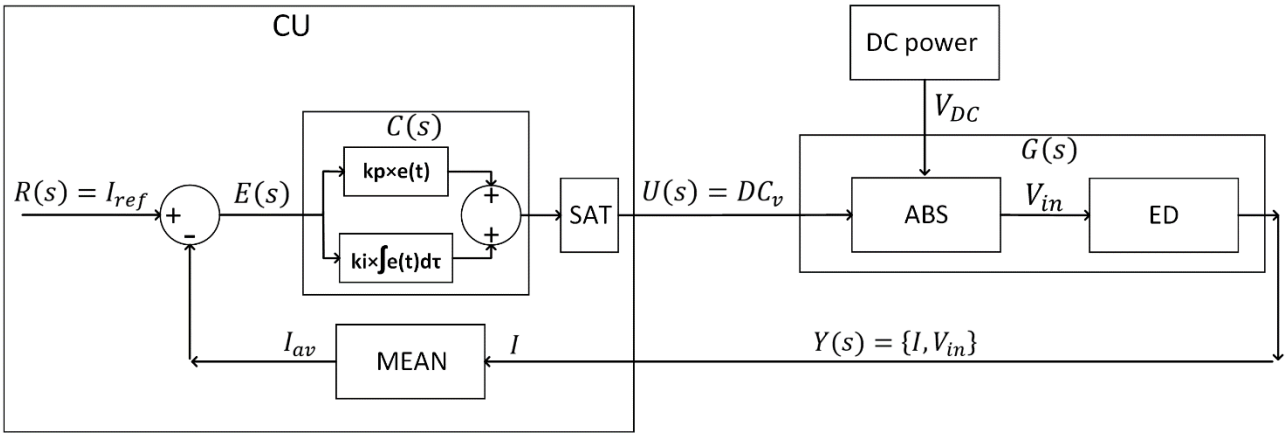

Figure 13: Electrodialysis setup with PI control integrated into the CU processing block.

The SAT block limits the operating range of DC_v to between 90% and 100%, as outside this range, the pEDR method does not show improvements in delaying fouling [28].

Although the plant G(s) provides the output $Y(s) = \{I, V_{in}\}$, the MEAN block only uses the current I, as it is the only signal from the two sensors available to obtain the average electric current I_{av} to be compared with the reference average electric current I_{ref}.

3.1.2 Stability of PI control

To demonstrate stability of the closed-loop with the transfer function of the $G(s)$ and the proposed controller $C(s)$, the nominal internal stability (theorem 3.1) lemma is applied [29] where the following expression must leave the roots in the left half-plane of Laplace domain to confirm convergence.

$$(s + \beta)s + \alpha(sK_p + K_I) = 0 \tag{3.3}$$

The obtained roots are:

$$s_{1,2} = \frac{\beta + \alpha K_p}{2} \pm i\frac{\sqrt{4\alpha K_I - (\beta + K_p)^2}}{2} \tag{3.4}$$

To keep the roots in the left half-plane, the following condition must be satisfied:

$$4\alpha K_I > (\beta + K_p)^2 \tag{3.5}$$

With a proportional gain K_p of 1 and an integral gain K_I of 268 for example, this condition is satisfied.

3.1.3 Simulation

The PI control is designed to impose a reference average current $I_{ref}(t)$ by acting on DC_v of the input voltage V_{in}. This is achieved by providing feedback from the current $I_{av}(t)$ obtained from measurements with the current sensor in the ED. As observed in figure 11, the average current $I_{av}(t)$ is obtained by sampling the current over time $I(t)$, precisely at the midpoint of each duty cycle, averaging the positive and negative values obtained from $I(t)$.

When $I_{ref}(t)$ is 0.9A, figure 14 illustrates how the PI control brings the average current $I_{av}(t)$ of the system from $0A$ (initial value) to $0.9A$, achieving this by increasing the duty cycle DC_v of the input voltage $V_{in}(t)$ from 50% to 80% in 0.2 seconds. In this case, the SAT block did not limit the DC_v so that the tracking of I_{ref} could be observed over a wide range.

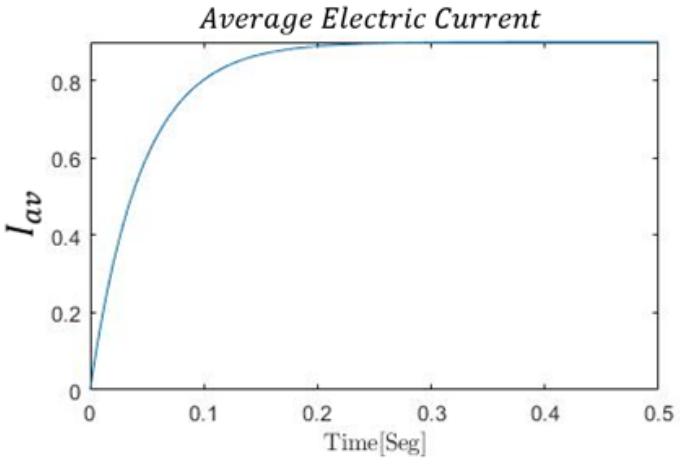

Figure 14: Simulated average electric current $I_{av}(t)$ in the ED starting from an initial value of $0A$ and reaching $0.9A$ to match the reference current $I_{ref}(t) = 0.9A$.

Thus, applying a PI control is sufficient for tracking $I_{ref}(t)$. However, there is still the task of implementing a supervisory control that changes the values of $I_{ref}(t)$ in such a way that fouling in ED is reduced. Therefore, within the same CU block, the processing of a supervisory control is integrated to take both sensors (I, V_{in}), observe changes in $R_{av}(t) = \frac{V_{in}(t)}{I(t)}$, and then impose an I_{ref} over time.

3.2 Extremum Seeking Control

So far, there is a PI controller that acts on the DC_v so that I_{av} can follow the reference I_{ref}. However, since we do not know all the parameters of the plant and do not know the optimal value of DC_v that ensures the ED fouls as slowly as possible, a supervisory block is added to the scheme (Figure 15). This supervisory block intelligently imposes new values of I_{ref} and includes advanced control that does not require a model of the plant (or at least not a direct one) and is also adaptive (in case the parameters that constitute the model of ED

changes over time). Taking the control scheme from figure 13, the supervisory block control block is added to meet the requirements, resulting in the new scheme shown in figure 15.

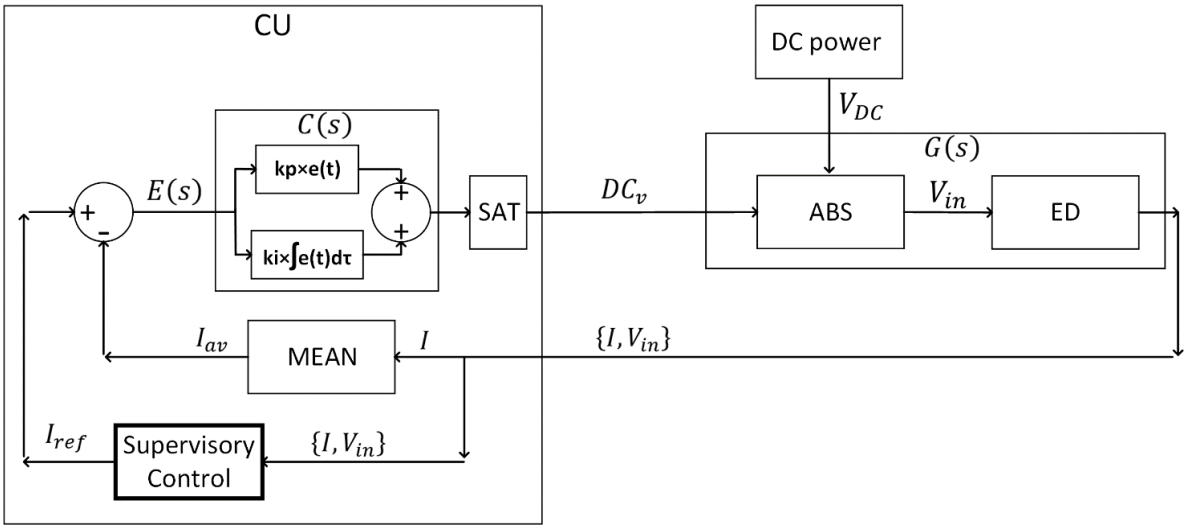

Figure 15: Electrodialysis setup with PI control and Supervisory Control integrated into the CU processing block.

Extremum Seeking Control (ESC) [27] are adaptive controllers that do not rely on a model and are useful for adapting to unknown system dynamics and unknown mappings from control parameters to an objective function.

ESC is applicable in situations where there is a nonlinearity in the control problem, and the nonlinearity has a local minimum or a maximum. The nonlinearity may be in the plant, as a physical nonlinearity, possibly manifesting itself through an equilibrium map, or it may be in the control objective, added to the system through a cost functional of an optimization problem. Hence, one can use extremum seeking both for tuning a set point to achieve an optimal value of the output, or for tuning parameters of a feedback law. The parameter space can be multivariable.

In this section, a fundamental theorem on Extremum Seeking [27] is used.

Theorem 3.2 *(Extremum Seeking) For the system in* figure 16*, the output error* $y - f^*$ *achives local exponential convergence to an* $O(a^2 + \frac{1}{w^2})$ *neighborhood of the origin provided the perturbation frequency w is sufficiently large, and* $\frac{1}{1+\frac{Kaf''}{2s}}$ *is asymptotically stable.*

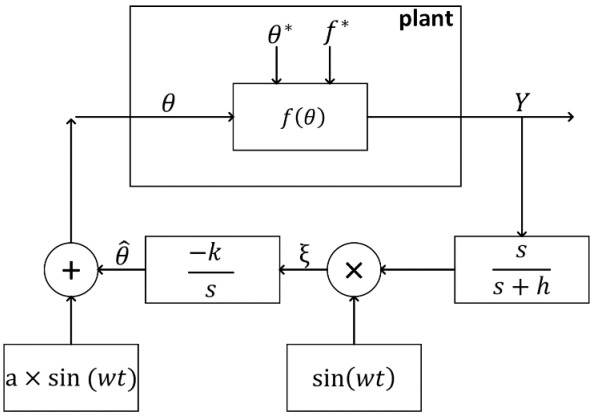

Figure 16: Basic Scheme of Extremum Seeking control for a static map with one variable for plant's input and output [27]

For a function with a static map, with $f^{"} > 0$ and for any C^2 function, the plant can be approximated by the function $f(\theta)$. The purpose of this algorithm is to make $\theta - \theta^*$ as small as possible, so that the output of $f(\theta)$ is driven towards its minimum f^*. The disturbance $asen(wt)$ is introduced to the plant to aid in measuring the information gradient of the map $f(\theta)$.

$$f(\theta) = f^* + \frac{f^{"}}{2}(\theta - \theta^*) \tag{3.6}$$

Then by noting that $\tilde{\theta}$ in figure 9 denotes the estimate of the unknown optimal input θ^*.

$$\tilde{\theta} = \theta^* - \hat{\theta} \tag{3.7}$$

Let denote the estimation error.

$$\theta - \theta^* = a\sin(wt) - \tilde{\theta} \tag{3.8}$$

Using the parabolic approximation, then gives:

$$y = f^* + \frac{f^{"}}{2}\left(\tilde{\theta} - a\sin(wt)\right)^2 \tag{3.9}$$

Expanding and using the trigonometric identity $2(\sin(wt))^2 = 1 - \cos(2wt)$:

$$y = f^* + \frac{f^{"}}{2}\tilde{\theta}^2 - af^{"}\tilde{\theta}\sin(wt) + \frac{a^2 f^{"}}{2}(\sin(wt))^2 \tag{3.10}$$

Then.

$$y = f^* + \frac{a^2 f^{"}}{4} + \frac{f^{"}}{2}\tilde{\theta}^2 - af^{"}\tilde{\theta}\sin(wt) + \frac{a^2 f^{"}}{4}\cos(2wt) \tag{3.11}$$

If $HPF = \frac{s}{s+h}$, applied to the output, serves to remove f^*:

$$\frac{s}{s+h}[y] \approx \frac{f^{"}}{2}\tilde{\theta}^2 - af^{"}\tilde{\theta}\sin(wt) + \frac{a^2 f^{"}}{4}\cos(2wt) \tag{3.12}$$

Then ξ is obtained with the demodulation for multiplying $\frac{s}{s+h}[y]$ with $\sin(wt)$:

$$\xi \approx \frac{f^{"}}{2}\tilde{\theta}^2\sin(wt) - af^{"}\tilde{\theta}(\sin(wt))^2 + \frac{a^2 f^{"}}{4}\cos(2wt)\sin(wt) \tag{3.13}$$

Using again the identity $2(\sin(wt))^2 = 1 - \cos(2wt)$ and $2\cos(2wt)\sin(wt) = \sin(3wt) - \sin(wt)$, it arrives at:

$$\xi \approx -\frac{af^{"}}{2}\tilde{\theta} + \frac{af^{"}}{2}\tilde{\theta}\cos(2wt) + \frac{a^2 f^{"}}{8}(\sin(wt) - \sin(3wt)) + \frac{f^{"}}{2}\tilde{\theta}^2\sin(wt) \tag{3.14}$$

Considering that θ^* is constant, it implies $\dot{\tilde{\theta}} = -\dot{\hat{\theta}}$. Then by multiplying with the integrator:

$$\tilde{\theta} \approx \frac{k}{s}\left[-\frac{af^{"}}{2}\tilde{\theta} + \frac{af^{"}}{2}\tilde{\theta}\cos(2wt) + \frac{a^2 f^{"}}{8}(\sin(wt) - \sin(3wt)) + \frac{f^{"}}{2}\tilde{\theta}^2\sin(wt)\right] \tag{3.15}$$

By neglecting the last term because it is quadratic in $\tilde{\theta}$:

$$\tilde{\theta} \approx \frac{k}{s}\left[-\frac{af^{"}}{2}\tilde{\theta} + \frac{af^{"}}{2}\tilde{\theta}\cos(2wt) + \frac{a^2 f^{"}}{8}(\sin(wt) - \sin(3wt))\right] \tag{3.16}$$

The last two terms are attenuated by the integrator:

$$\tilde{\theta} \approx \frac{k}{s}\left[-\frac{af^{"}}{2}\tilde{\theta}\right] \tag{3.17}$$

Then.

$$\dot{\tilde{\theta}} \approx -\frac{kaf^{"}}{2}\tilde{\theta} \tag{3.18}$$

Since $kaf^{"} > 0$, this is a stable system.

$$\tilde{\theta} = e^{-\frac{kaf^{"}t}{2}} \tag{3.19}$$

When $t \to \infty$ implies that $\tilde{\theta} \to 0$.

$$\lim_{t\to\infty} e^{-\frac{kaf^{"}t}{2}} = 0 \tag{3.20}$$

That's mean $\hat{\theta}$ converges to a small distance of θ^*. Since $kf^{"} > 0$ this is a stable system. This approximation holds only when w is large (in a qualitative sense) relative to k, a, h and $f^{"}$.

3.2.1 Objective function

In this work the use of ESC allows, through its adaptive capacity, to compensate for the fact that the exact influence of flow, pressure, pH, conductivity, and temperature on the mathematical model describing the ED is unknown.

The goal is to influence the V_{in} to the ED system, with the purpose of observing improvements in terms of reducing fouling growth on the ion exchange membranes of the system [22], this growth of fouling can be measured by the variation in the average electrical resistance ($\dot{R}_{av}$) of the ED. The higher the $\dot{R}_{av}$, the faster the fouling grows.

Following this, convergence to the optimal point (where system fouling grows more slowly) is demonstrated. Finally, the simulation results employing ESC with PI in cascade to determine if the system, as it changes the DC_v, manages to reduce the growth of fouling.

First, to propose the controller design, it is important to simplify the mathematical model of the ED. This pertains to the resistance related to fouling Z_T.

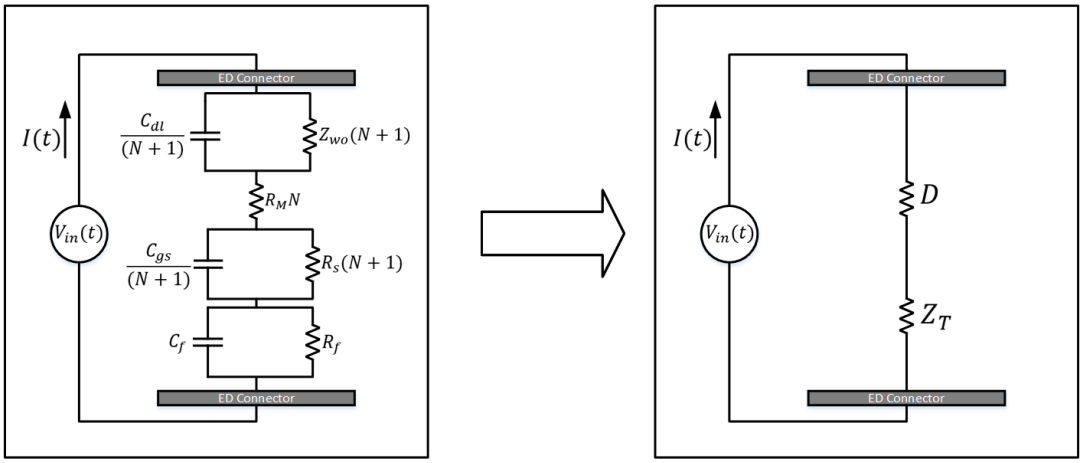

Figure 17: According to [10], Simplified equivalent circuit: Z_{wo} represents the Warburg impedance in the electrical double layer (EDL); C_{dl} represents the electric double layer capacitance (EDL); R_M represents the resistance of the ion exchange membrane (IEM); R_s represents the resistance of the diffusion boundary layers (DBL); C_{gs} represents the capacitance of the diffusion boundary layers (DBL); and V_{in} represents the voltage supply. Then, according to the simplification, Z_T represents the fouling resistance. Finally, for control purposes, Z_{wo}, C_{dl}, R_s, C_{gs}, and R_M are approximated to a constant D.

The motivation for proposing this new mathematical structure for Z_T is to integrate into a proposed control, an objective function that allows achieving a global minimum. In this case, it would be the moment when fouling resistance grows slowest by applying a DC_v and a fixed frequency of 4k hertz the input voltage V_{in} that enables the discovery of this global minimum.

There is the growth of the average resistance over time, caused by fouling with organic and inorganic matter on the walls of the ion exchange membranes [22]. This effect is evidenced by the nonlinear component Z_T, which mainly depends on the DC_v and the frequency of the input voltage to the ED. Additionally, it depends on temperature, pH, flow rate, conductivity, and material properties of the ED in unknown proportions. However, based on experiments associated with the publication [22] [17], as an approximation the waveform representing the growth of electrical resistance over time is expressed as a mathematical function of parameters with unknown magnitudes, generalized in (3.21).

$$Z_T = Ae^{\frac{t}{\tau C}} - Be^{\frac{-t}{\tau}} \tag{3.21}$$

Considering the average resistance for the rest of the circuit (D) and adding the fouling resistance (Z_T), (3.22), (3.23), and (3.24) are obtained.

$$R_{av}(t) = Z_T + D = Ae^{\frac{t}{\tau C}} - Be^{\frac{-t}{\tau}} + D \tag{3.22}$$

$$\dot{R}_{av}(t) = \frac{A}{\tau C}e^{\frac{t}{\tau C}} + \frac{B}{\tau}e^{\frac{-t}{\tau}} \tag{3.23}$$

$$\ddot{R}_{av}(t) = \frac{A}{(\tau C)^2}e^{\frac{t}{\tau C}} - \frac{B}{\tau^2}e^{\frac{-t}{\tau}} \tag{3.24}$$

The global minimum of $\dot{R}_{av}(t) = \frac{d}{dt}(D + Z_T(t))$ as seen in figure 18 when $t = T_{in}$.

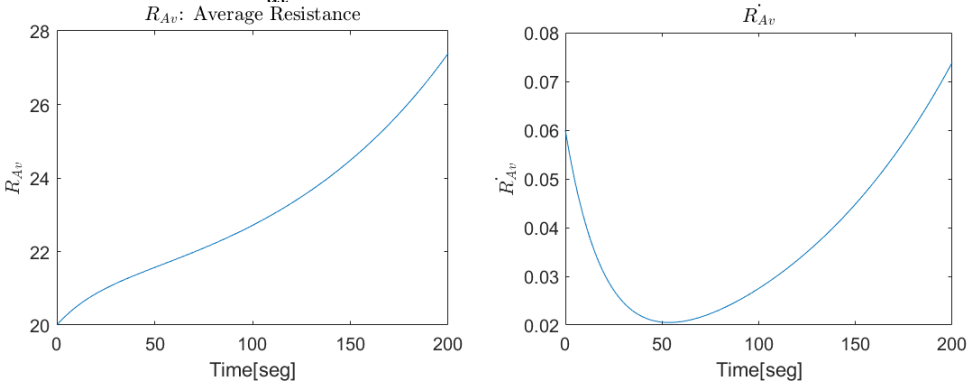

Figure 18: $R_{av}(t)$: Approximation of System Resistance over time, obtained from [22](Experiment T0). $\dot{R}_{av}(t)$: Derivative of the Average Resistance with a global minimum.

From figure 18, the inflection point is obtained at $T_{in} = 53.65$ seconds $\rightarrow \ddot{R}_{av} = 0$, with an initial value of 20Ω, and after 200 seconds, a value of 27.3 Ω for the stack of 10 ion exchange membranes that constitute the ED.

The parameters are $A = 1$, $B = 1$, $C = 5$, $D = 20$ y $\tau = 20$ According to the experiments on [22].

In (3.21), representing the resistance due to fouling in the complete stack of IEMs ($Z_T(t)$), is derived from the sum of exponentials with parameters A, B, C, and τ. The values of these parameters are obtained from experiment T0 [22], where a constant voltage of $V_{in} = 23V$ was applied to the electrodialyzer terminals.

If the voltage (V_{in}) at the electrodialyzer terminals is asymmetrically pulsed using the pEDR method (pulsed Electrodialysis Reversal), the amplitude of the fouling-induced resistance ($Z_T(t)$) grows more slowly than when applying a constant voltage V_{in} to the electrodialyzer terminals.

Considering the above, it can be generalized that Z_T grows more slowly or faster depending on the DC_v and the frequency of the applied voltage (V_{in}) to the ED terminals. Therefore, by varying the values of DC_v and/or the frequency in the voltage V_{in}, the parameters A, B, C, and τ change.

The simplifications made, such as the temperature, pH, flow in the input and output flow rates, conductivity and material properties of the ED, do not affect the parameters A, B, C, and τ of $Z_T(t)$. Therefore, only the DC_v and the frequency of V_{in} can change the values of the parameters A, B, C, and τ.

The constant D is obtained from the Average Resistance representing the circuit without fouling. Its value is obtained from the sum of $R_M N$, $R_s(N+1)$, and $Z_{wo}(N+1)$, which is approximately 20Ω (exactly 18.7993Ω) in the experiments of reference [22]. Capacitances C_{dl} and C_{gs} are not considered in this analysis since their electrical contribution is not significant for the analysis of this work (they are not related to the

average system resistance, nor do they alter the growth of resistance due to fouling).

Finally, the average resistance of the ED system ($R_{av}(t)$) is obtained by summing the constant D (representing the fouling-free electrodialyzer model) and the fouling resistance Z_T resulting in (3.22), (3.23), and (3.24).

In this study, $\dot{R}_{av}(t)$ has a global minimum, representing the moment when the average system resistance $R_{av}(t)$ grows at the slowest rate. Therefore, the objective of this work is to reach this global minimum by acting on the DC_v of the input voltage (V_{in}) at a fixed frequency, and this function $\dot{R}_{av}(t)$ is going to be the objective function of the ESC scheme.

V_{in} is always a signal with the pEDR method, therefore it has a frequency, positive and negative amplitude of constant magnitude, and DC_v. Then we obtain the average value of the electric current $I(t)$ and the voltage V_{in} to obtain $R_{av}(t)$ by applying Ohm's law. Having the average electric current $I_{av}(t)$ and feedback to the system, which aims to change the DC_v using PI control , it is necessary for ESC to impose a reference average electric current $I_{ref}(t)$, so that this reference enters a PI control and it finds the DC_v in order to obtain said average electric current $I_{av}(t)$ equal to $I_{ref}(t)$.

The goal is:

Figure 19: Flowchart of the Purpose of the Proposed Controller.

3.2.2 Proposed cascade connection of ESC & PI control

Using the structures from figure 15 and figure 16, to ensure that an objective function $\dot{R}_{av}$ is obtained from the sensors I and V_{in}, and processed to reach an I_{ref} that finds the minimum of $\dot{R}_{av}$ ($\dot{R}_{av}{}^{*}$), the structure of the ESC, including the OBJECTIVE FUNCTION block, is introduced within the supervisory block.

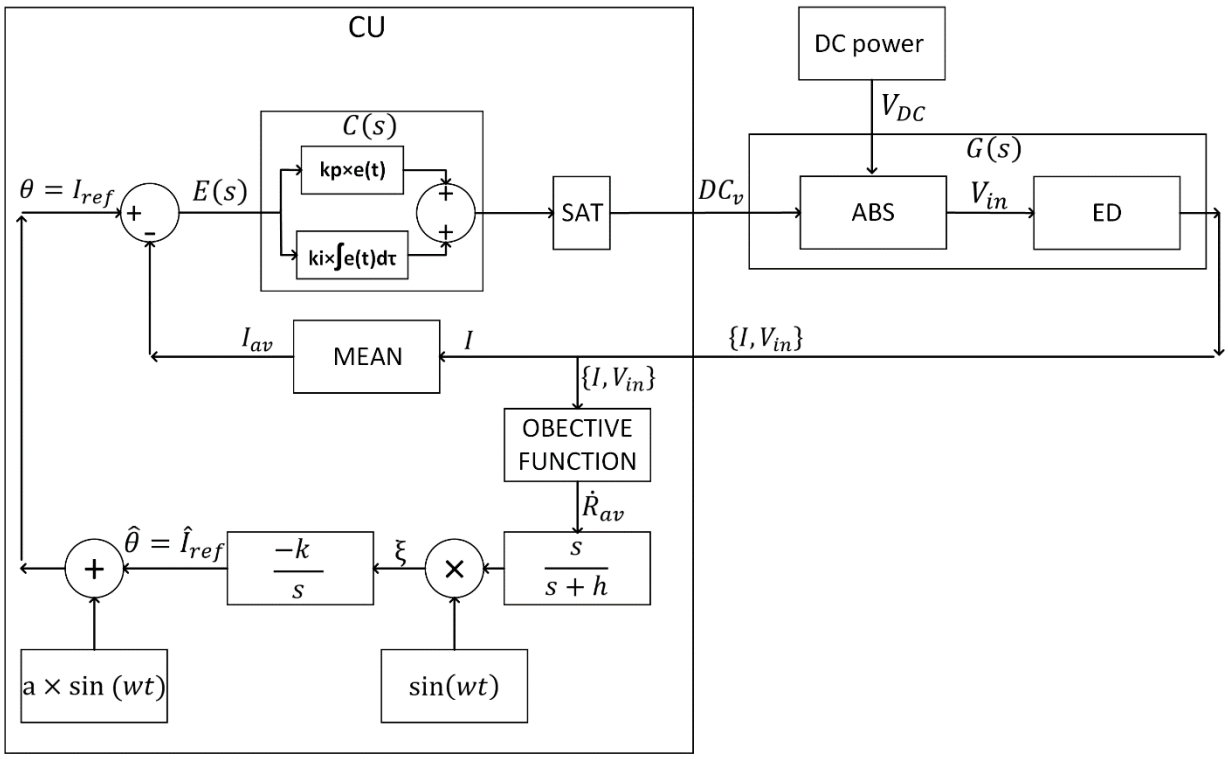

Figure 20: Electrodialysis setup with ESC cascade with PI control integrated into the CU processing block.

The new additions on this control scheme can be observed in figure 20:

- ξ: Magnitude of the error around the Global Minimum $\dot{R}_{av}{}^{*}$ of the Objective Function $\dot{R}_{av}$.
- $\frac{s}{s+h}$: First-order high-pass filter to eliminate the mean value and only obtain the variation around zero of the $\dot{R}_{av}$.
- $OBJECTIVE\ FUNCTION$: With samples of the input voltage $V_{in}(t)$ and electric current $I(t)$, weighted over time $\dot{R}_{av}(t)$ is obtained.
- $a \times \sin(wt)$: sine wave perturbation to I_{ref}, to explore whether a higher or lower value of I_{ref} results in an improvement in $\dot{R}_{av}$.
- $\sin(wt)$: sine wave perturbation, to demodulate whether the positive or negative perturbation of I_{ref} generated a positive or negative perturbation in $\dot{R}_{av}$.Then, if this multiplication $I_{ref} \times \dot{R}_{av}$ is positive or negative, ESC can determine whether it should increase or decrease to approach the global minimum $\dot{R}_{av}{}^{*}$.
- $\frac{-k}{s}$: First-order integrator with gain k negative, to add the error ξ around $\dot{R}_{av}{}^{*}$. Therefore, if the accumulated error by the integrator is very high (whether positive or negative), the value of I_{ref} should increase or decrease more rapidly to approach $\dot{R}_{av}{}^{*}$. On the other hand, if the accumulated error in the integrator is small and oscillates between a positive and negative value, it means that it is near the global minimum $\{I_{ref}{}^{*}, \dot{R}_{av}{}^{*}\}$.

Its step-by-step mathematical operation is (Figure 20):

1. First, by applying DC_v in the input voltage V_{in} of the electrodialysis system, this imposes a reference average current $I_{ref}(t)$. That is, if a $DC_v = 95\%$, for example, a reference average current is obtained:

$$I_{ref}(\mathrm{t}) = DC_v \times |I_{positive}| - (1 - DC_v) \times |I_{negative}| = 0.95 \times |I_{positive}| - 0.05 \times |I_{negative}| \quad (3.25)$$

   Where $I_{positive}$ is the electric current $I(t)$ obtained with a current sensor when the voltage V_{in} is positive, and $I_{negative}$ is the electric current $I(t)$ obtained with a current sensor when the voltage V_{in} is negative. So, if $I_{positive} = 1A$ and $I_{negative} = -1A$ for example, the reference average current is going to be $I_{ref}(t) = 0.9A$. To impose a desired reference average current $I_{ref}(t)$ on the electrodialyzer, a simple PI control is used, which varies the value of DC_v of the input voltage V_{in} to maintain the desired $I_{ref}(t)$ in the ED.

2. With the previous step, it can be ensured that the ED has a desired average electric current $I_{av}(t)$. Then, the ESC must intelligently impose the reference average current $I_{ref}(t)$ on the electrodialyzer in such a way as to obtain the slowest possible growth of the average resistance $R_{av}(t)$. To achieve this goal, the variation of the average resistance over time $\dot{R}_{av}(t)$ is obtained. If the variation is very high, it means that the resistance has grown a lot, and it is imperative to change the value of the reference average current $I_{ref}(t)$, so that $\dot{R}_{av}(t)$ has small variations, and so on.

3. To achieve the goal of step 2, the value obtained from $\dot{R}_{av}(t)$ is disturbed with sinusoidal signals, multiplied by a high pass filter and then an integrator, which are the necessary mathematical tools to vary the amplitude of $I_{ref}(t)$ and make $\dot{R}_{av}(t)$ converge to the smallest possible variations (implying the slowest possible growth of the average resistance $R_{av}(t)$ due to fouling in the IEMs).

Understanding the logic behind the cascade connection between ESC and PI control, the values of the parameters for the PI and ESC controllers are obtained.

The issue is that, depending on the operating conditions, T_{in} varies over time. In other words, the control acts by delivering a reference average current $I_{ref}(t) = \theta$. Then, through the PI control, DC_v feeding the ED plant is obtained. Finally, through an objective function, which analyzes the variation of the average resistance $\dot{R}_{av}(t)$, passing through a high-pass filter to eliminate readings outside the expected frequency range, it is multiplied by a sinusoidal signal with amplitude and frequency configured with respect to the plant's dynamics. The values of the parameters defined in figure 20 are: a = 0.0025, w = 0.1 rad/s and the gains of the PI Control are $k_p = 1$ and $k_i = 268$.

The amplitude of $a = 0.0025$ since the known operating range of the reference current $I_{ref}(t)$ in this study is from $0A$ to $1.5A$, given the operating limitations of the pEDR method. $I_{ref}(t)$ can only have values between $1.35A$ to $1.5A$ since DC_v ranges from 90% to 100% (SAT block). If a were a very high value, $I_{ref}(t)$ would saturate at $1.35A$ or $1.5A$.

The bandwidth of HPF is 1 rad/s since the dynamics of the plant are slower than the growth of the average resistance $R_{av}(t)$ (in the order of minutes) and is also 10 times larger than w (sinusoidal perturbation) to avoid filtering out the contribution of the perturbation to the input signal I_{ref}.

The value of w is 0.1 rad/s given the slow dynamics of the plant, which shows changes in $R_{av}(t)$ at intervals greater than 10 seconds.

It is assumed that the time for obtaining the average resistance $R_{av}(t)$ is not relevant to the frequency at which the ESC operates, as obtaining a sample of $V_{in}(t)$ and $I(t)$, which are then divided to obtain $R_{av}(t)$, is in the order of microseconds.

Similar to how it controls with ESC in an electrolysis system [32] or hall-héroult aluminium process [33]

with only one input and one output to a function with a unique global minimum that is desired to be found, its convergence is demonstrated in the simulations of chapter 3.3.3.

Where the objective function of the system ($\dot{R}_{av}(t)$)must converge to $\dot{R}_{av}{}^{*} = \frac{A}{\tau C}\left(\frac{BC^2}{A}\right)^{\frac{1}{C+1}} + \frac{B}{\tau}\left(\frac{BC^2}{A}\right)^{\frac{-C}{C+1}} \approx 0.02\frac{\Omega}{sec}$, which is obtained in figure 18. The value to which the objective function $\dot{R}_{av}(t)$ must converge is obtained by evaluating it at the inflection point where $\ddot{R}_{av}(t) = 0$ (with the parameters $A = 1$, $B = 1$, $C = 5$ y $\tau = 20$).

3.3.3 Stability of cascade connection of ESC & PI control

Before demonstrating the convergence to the global minimum of the system, the following two simplifications are made.

1) It is assumed that the PI control, which takes an $I_{ref}(t)$ and outputs a DC_v, is simply a gain, given that the dynamics of the ESC controller are slower compared to the PI control.

2) In accordance with figure 20, the C(s) (now considered a gain), the G(s), and the objective function block are reduced to a single block, which is fully represented by the variation of average resistance growth function $\dot{R}_{av}$(t).

Taking into consideration the two mentioned simplifications, the convergence to the global minimum of the function is demonstrated using the method outlined in the chapter one of the book [27] (Theorem 3.2) for a static map with one input and one output.

First, by considering the function of the variation of average resistance growth function $\dot{R}_{av}$(t), which possesses an exponential mathematical structure presented in (3.23), in the vicinity of its global minimum $\left(I_{ref}{}^{*}, \dot{R}_{av}{}^{*}\right)$, it can be approximated by a parabolic function with the following structure:

$$\dot{R}_{av}(I_{ref}(t)) = \dot{R}_{av}{}^{*} + \frac{\dot{R}_{av}{}^{"}}{2}\left(I_{ref}(t) - I_{ref}{}^{*}\right)^2 \tag{3.26}$$

With the constant $\dot{R}_{av}{}^{"} > 0$.
Then by noting that $\tilde{I}_{ref}(t)$ in figure 20 denotes the estimate of the unknown optimal input $I_{ref}{}^{*}$.

$$\tilde{I}_{ref}(t) = I_{ref}{}^{*} - \hat{I}_{ref}(\mathrm{t}) \tag{3.27}$$

Using the same demonstration of Theorem 3.2, we obtain.

$$\lim_{t\to\infty} e^{-\frac{KA\dot{R}_{av}{}^{"}t}{2}} = 0 \tag{3.28}$$

That's mean $\hat{I}_{ref}(t \to \infty)$ converges to a small distance of $I_{ref}{}^{*}$. Therefore, the control ESC with PI Control in cascade connection applied to this plant is going to find its global minimum ($\dot{R}_{av}{}^{*}$).

3.2.4 Simulation

Using the controller defined in figure 20 the figure 21 and figure 22 are obtained.

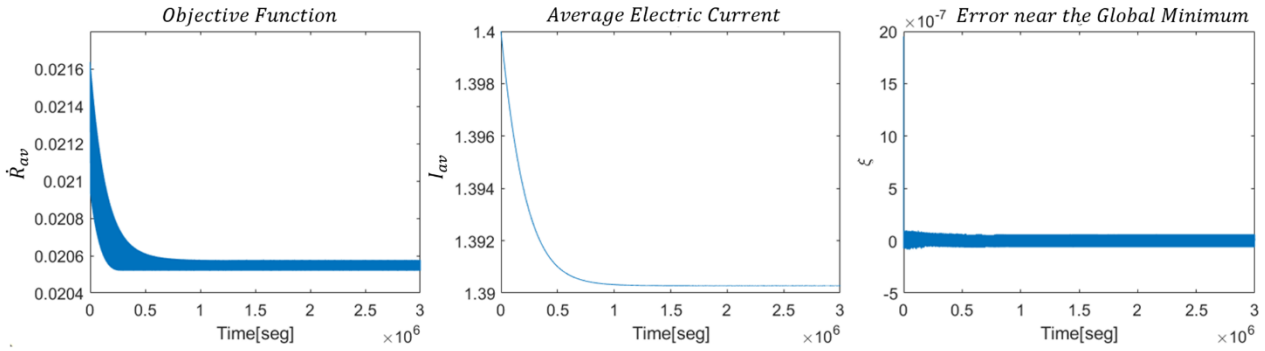

Figure 21: $\dot{R}_{av}(t)$: Variation of simulated electrical resistance in the ED; I_{av}: Simulated electric current $I_{av} = I_{ref}$ in the ED; ξ: Variation of the error around the global minimum.

$$DC_v = \frac{I_{ref(t)}}{MAX_I} - 0.9 \tag{3.29}$$

From (3.29), MAX_I is the maximum value that the reference current $I_{ref}(t)$ can reach ($MAX_I = 1.5A$) and from figure 21, the optimal performance of $I_{ref}(t)$ is when it has a value of $1.3915A$, implying a $DC_v = 92.6\%$ and a variation of average resistance $\dot{R}_{av} = 0.02\ \Omega/s$.
The error moves around zero ξ with low amplitude, implying that the system converges to the global minimum (pair: ${I_{ref}}^* = 1.3915\ A, {\dot{R}_{av}}^* = 0.02\ \Omega/s$).

An initial value of $I_{ref} = 1.4A$ was applied. It is known that A, B, C and τ vary over time, but in this case, they were analyzed as if they were a static map (constant).

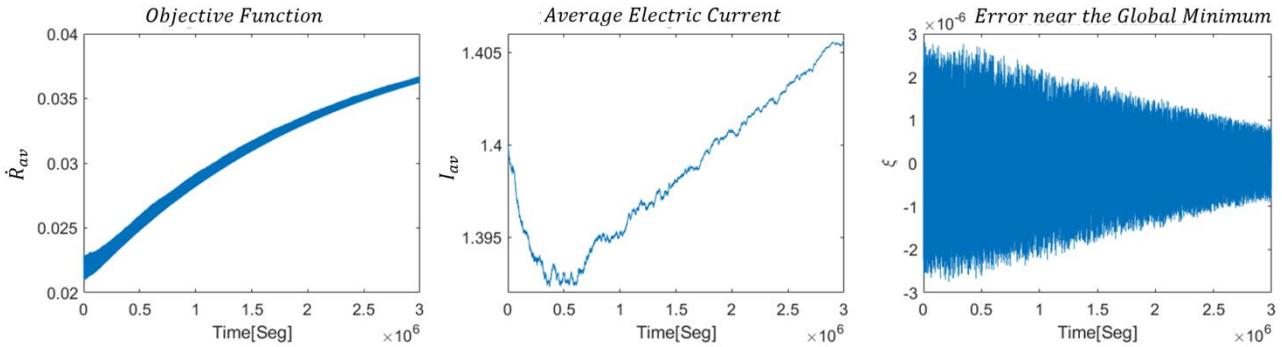

Figure 22: $\dot{R}_{av}$(t): Variation of simulated electrical resistance in the ED; I_{av}: Simulated electric current $I_{av} = I_{ref}$ in the ED; ξ: Variation of the error around the global minimum. *A, B, C and τ Disturbed by (3.30).*

As seen in figure 22, $R_{av}(t)$ will be varying its parameters A, B, C and τ, multiplying each one by (3.30). This variation will always be increasing (as observed in the experiments in the article [22]). Therefore, the control over the system is simulated considering that A, B, C and τ grow slowly and with disturbances from unknown proportions given by temperature, pH, flow, conductivity and materiality.

It can be observed that, despite the variation of A, B, C and τ over time and in an increasing manner, the ESC in cascade with a PI control is able to track the global minimum of the objective function $\dot{R}_{av}$(t), which increases over time.

$$\rho = 6.66 \times 10^{-7} t + u + \sum \tag{3.30}$$

In (3.30), μ and Σ are the mean and variance of a Gaussian distribution, with values of 0 and ~ 0.1, respectively. $6.66 \times 10^{-7} t$ represents the slow linear growth.

For simplification, when simulating the control scheme, it is assumed that the PI is simply a proportional conversion, instantly converting a reference current $I_{ref}(t)$ into a DC_v, so $I_{ref} = I_{av}$. This assumption is made considering that the convergence times of the PI Control are on the order of $1\ second$, as seen in the previous subsection, which is negligible compared to the convergence times of ESC.

Another simplification is that the plant instantly delivers sampled values of $V_{in}(t)$ and $I(t)$ since this sampling is on the order of microseconds to obtain $R_{av}(t)$, which is insignificant for the operating times of ESC.

Chapter 4

Experimental validation on a pilot plant

Primarily, the list of hardware and firmware utilized for conducting the experiments is presented. To demonstrate the functionality of the controller to be implemented, the same logic as in the simulations is followed. Initially, it is verified that the PI Control can effectively track a reference average current I_{ref}, even under extreme conditions. Subsequently, tests are conducted by connecting the ESC with the PI in cascade, aiming to observe whether the system attempts to seek the unknown global minimum of the average electrical resistance variation function $\dot{R}_{av}(t)$.

The test to be conducted with the ABS in conjunction with the ED pilot plant is to demonstrate that the ABS, which until now has only been tested at the laboratory level [28] (under 20 W), is capable of functioning at an industrial level (with power levels reaching 30KW) and has the ability to operate in two modes. One mode allows the user to manually input the DC_v voltage and frequency to act on ED directly, and the other mode enables an adaptive ESC control in cascade with PI control to slow down fouling. This project is a collaboration between AC3E and ARAUCO-BIOFORES of Concepción, Chile.

It is expected that the results will enhance the use of this technology (Electrodialysis) for cleaning contaminated water, which is a byproduct of the KRAFT process, instead of using Reverse Osmosis, which has higher energy consumption to do the same task, water desalination.

Figure 23: Left: ED pilot plant. Right: ABS (designed in AC3E).

4.1 Applied Equipment, Hardware and Firmware

To run the proposed control system a Texas Instruments TMS320F28379D microcontroller is used. It employs 4 PWM channels from this microcontroller to act on 4 UCC21732-Q1 Gate Drivers. Each gate driver is responsible for controlling a power MOSFET to switch a voltage from a DC source (Figure 9), allowing the generation of a variable frequency and duty cycle voltage pulse train (with pEDR method). Additionally, 2 analog inputs of the microcontroller are enabled to obtain readings of voltage and electric current amplitude applied to the electrodialyzer ($V_{in}(t)$ and $I(t)$). All the mentioned hardware and firmware components together constitute the asymmetric bipolar switch (ABS).

With the hardware, the control logic mentioned in the previous chapter is programmed. Having voltage and electric current readings enables the generate a control loop, as explained in chapters 3.1 and 3.2.

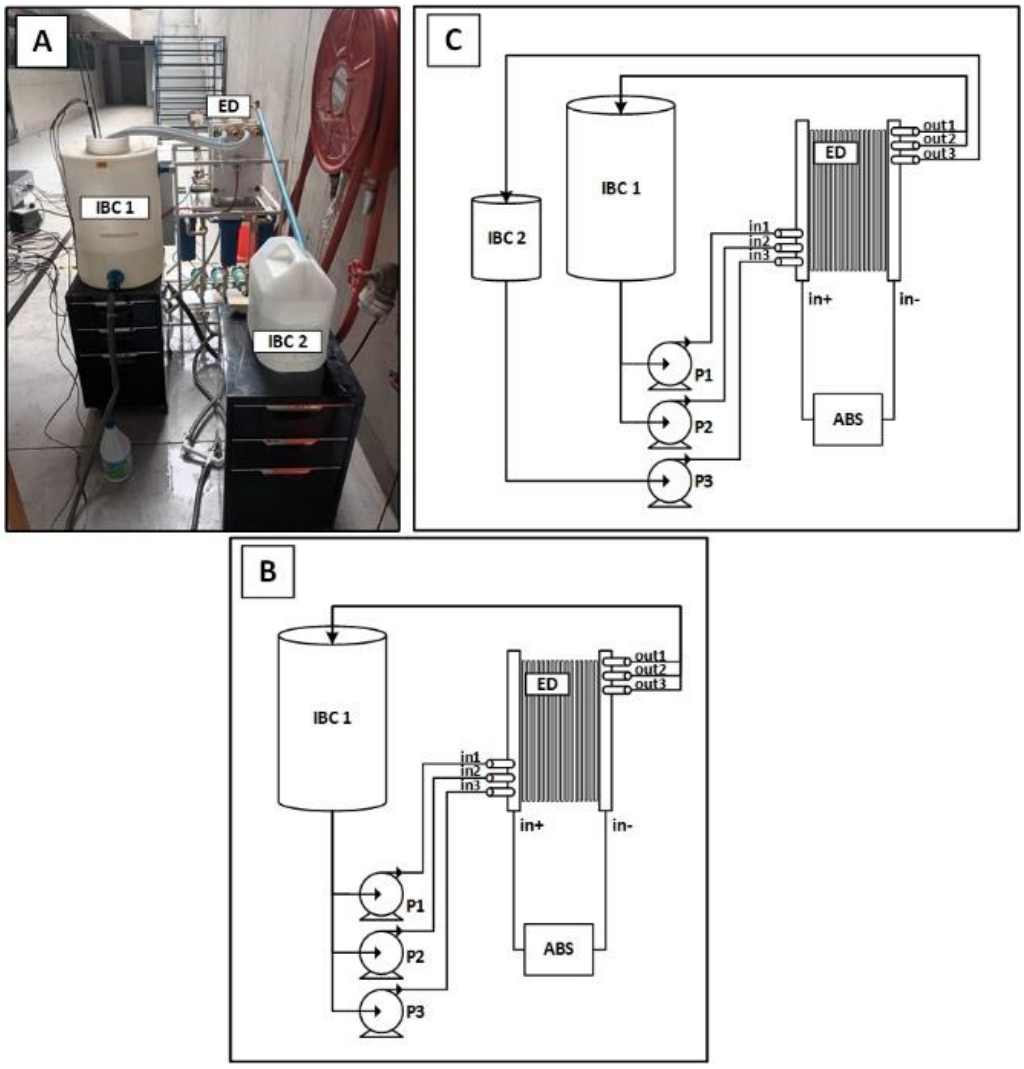

Figure 24: ED Equipment: A) Image of the real equipment to be used at the AC3E facilities. B) Hydraulic connection for performing PI control tests. C) Hydraulic connection for performing ESC cascade with PI control tests.

Item	Description	Sensors	Observations
IBC1	60 liter storage tank.	Temperature and Conductivity.	Located 45cm above pumps P1, P2, and P3.
IBC2	20 liter storage tank.	-	Located 45cm above pumps P1, P2, and P3.
ED	Electrodialysis Pilot Plant.	Electric Current and Voltage.	Electrodialyzer with 10 pairs of ion exchange membranes.
P1	Centrifugal pump for pumping diluted solution to the ion exchange membranes of the ED unit.	-	3/4 HP
P2	Centrifugal pump for pumping concentrate to the ion exchange membranes of the ED unit.	-	3/4 HP
P3	Centrifugal pump for pumping saline solution to the electrodes of the ED unit.	-	3/4 HP
in1	Inlet of diluted solution to the ion exchange membranes of the ED unit.	Flow and Pressure.	-
in2	Inlet of concentrate to the ion exchange membranes of the ED unit.	Flow and Pressure.	-
in3	Inlet of saline solution to the electrodes of the ED unit.	Flow and Pressure.	-
out1	Outlet of diluted solution from the ED unit.	-	-
out2	Outlet of concentrate from the ED unit.	-	-
out3	Outlet of saline solution from the electrodes of the ED unit.	-	-

Table 5: Electrodialysis Unit (ED) for conducting experimental tests.

4.2 Test #1: PI Control

Only the PI control is tested, without adding whey protein, to ensure there is no increase in resistance due to fouling and only test if I_{av} can follow I_{ref}.

Is explained how tests were conducted using the complete PI Control scheme proposed in figure 13. The PI Control is responsible for acting on DC_v of the input voltage $V_{in}(t)$ of the ED to obtain an average electric current $I_{av}(t)$ (after MEAN block figure 13) with a fixed frequency of $4\,KHz$, the microcontroller takes 100 samples in a period identical to the frequency of the input voltage $V_{in}(t)$. This is because it samples (collects data) of voltage and electric current right in the middle between $V_{in}(t)$ switches.

So, if the frequency of $V_{in}(t)$ is $4\,kHz$, that means an average electric current $I_{av}(t)$ is obtained every $0.0125\ seconds$. This is because it captures a positive electric current amplitude and a negative electric current amplitude of $I(t)$ in a period of $1/4000\ seconds$. Then, the average of these positive electric currents $I_{positive}$ and negative electric currents $I_{negative}$ is related to the current duty cycle DC_v, and the average electric current $I_{av}(t)$ is obtained as follows:

$$I_{av} = DC_v \times \left|I_{positive}\right| - (1 - DC_v) \times |I_{negative}| \tag{4.1}$$

For the PI Control test, we work with an output voltage amplitude from the ABS to the ED of 30.5 Vdc, set the switching frequency to 4 kHz, and use the configuration in figure 24B with the IBC1 tank at a concentration of 7000 $\mu S/cm$.

The DC_v is limited to a range of 70% to 96% because it is not of interest to analyze control outside these operating range. The ED delivers 1.5 $Amperes$ at a constant input voltage of 30.5 Vdc; therefore, at a DC_v of 70% (using (4.1)), it corresponds to an average electric current $I_{av}(t)$ of 0.6 $Amperes$, and at a DC_v of 96%, it corresponds to an average electric current $I_{av}(t)$ of 1.38 $Amperes$.

The test was carried out for 11 $minutes\ and$ 38 $seconds$, during which the following tests were conducted.

I_{ref} [A]	I_{av} [A]	Duration [s]	Observations
1.35	1.36 ± 0.026	221	-
0.9	0.91 ± 0.021	177	-
1.4	1.41 ± 0.021	181	-
0.65	0.67 ± 0.010	119	An average slightly further from the reference value is observed, this is due to the overshoot (a peak in the average electrical current) when changing the value of the reference current I_{ref}.

Table 6: PI control results.

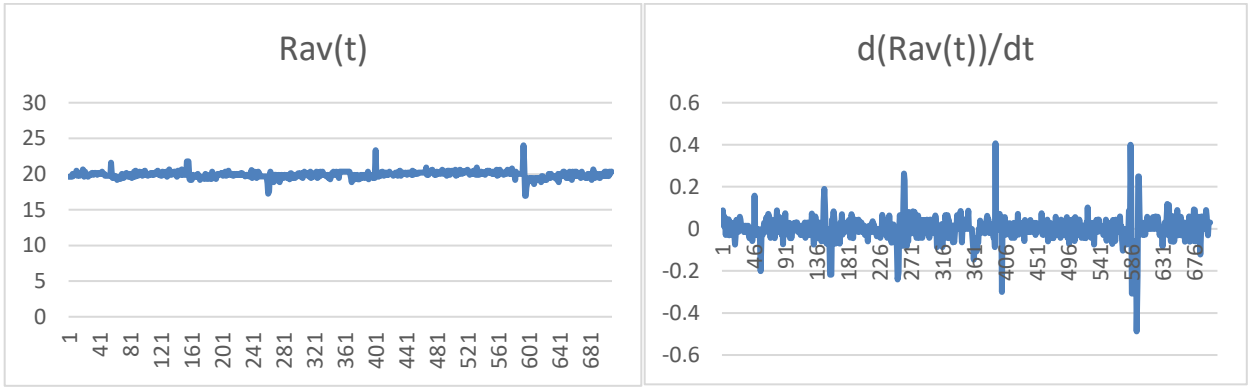

Figure 25: Left: Electrical resistance of the system $R_{av}(t)$ over time when applying pEDR voltage with no fouling, Right: Variation in electrical resistance of the system $\dot{R}_{av}(t)$ over time when applying pEDR voltage with no fouling.

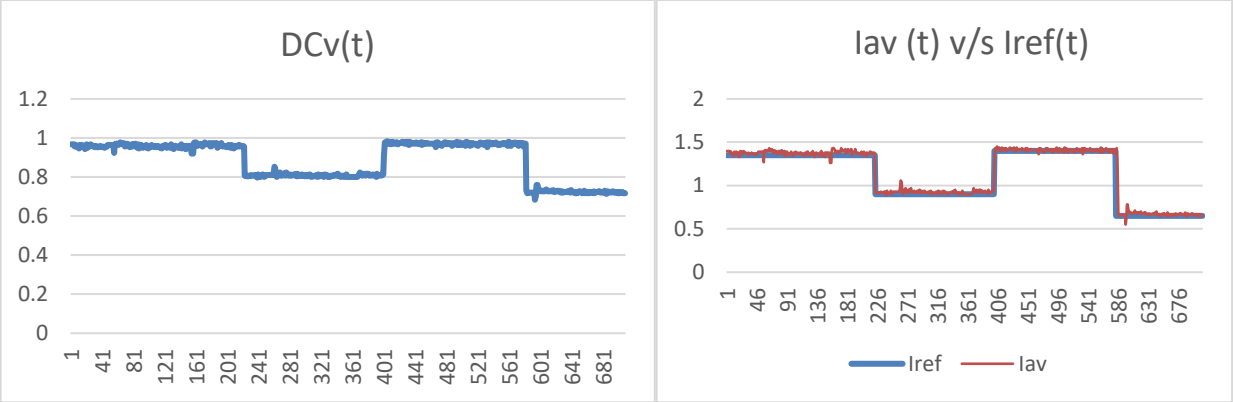

Figure 26: PI control result of the average electrical current $I_{av}(t)$ following the reference electrical current $I_{ref}(t)$.

It can be observed that the average current I_{av} can follow the reference current I_{ref} with little error under 10% (Table 6). Additionally, the average resistance R_{av} of the ED remains constant since there is no organic matter (whey protein) in the system.

4.3 Test #2: Constant Voltage Without Control.

To carry out Test#2 the system is tested without control usage (without switching the voltage by the ABS), using the plant scheme in figure 24C and adding whey protein to observe the membrane fouling and its fouling resistance increase $R_{av}(t)$ (with organic matter). Then, the plant is cleaned with caustic soda.

A step-by-step description is provided on how the tests were conducted using constant voltage at the terminals of the ED and adding whey protein.

1. A constant input voltage of 23 Vdc was applied to the electrodes of the ED, and the electrical current $I(t)$ and input voltage $V_{in}(t)$ were recorded during an 800 $second$ trial.

2. The test was conducted with a mixture previously prepared in IBC 1, containing 20 $liters$ of water, 200 $grams$ of whey protein, and 95 $grams$ of table salt, to ensure that there is sufficient conductivity and fouling for the purpose of this study, the proportions are obtained from [34]. The mixture was left with a conductivity close to 6000 $\mu S/cm$.

3. A submersible pump was kept active inside IBC 1 to maintain homogeneous mixing.

4. IBC 2 was kept with a conductivity of 6000 $\mu S/cm$ to circulate liquid without proteins from IBC 1 to the ED electrodes.

5. During the test, the variation of electrical resistance $R_{av}(t)$ and the rate of change of electrical resistance $\dot{R}_{av}(t)$ of the ED system over time were recorded.

6. Figure 27 shows the results of the test, indicating that the system's resistance $R_{av}(t)$ increased from 27.6 Ω to a maximum of 28.7 Ω and the variation in resistance $\dot{R}_{av}(t)$ stabilizes at a value close to 0.005 $\frac{\Omega}{seg}$. Additionally, an increase in the mixture's temperature from 17.2°C to 19.5°C was recorded during the 800 $seconds$ of the test.

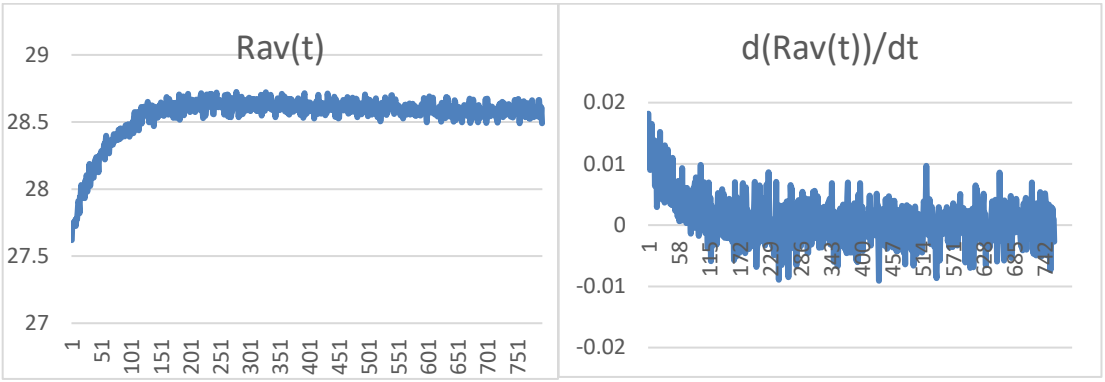

Figure 27: Left: Electrical resistance of the system $R_{av}(t)$ over time when applying constant voltage, Right: Variation in electrical resistance of the system $\dot{R}_{av}(t)$ over time when applying constant voltage.

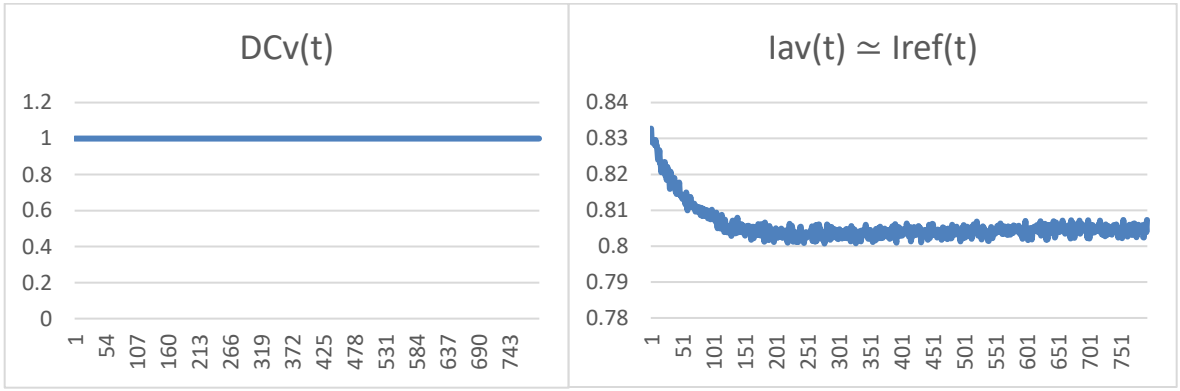

Figure 28: Left: Duty cycle DC_v of the input voltage over time in the system when applying constant voltage. *Right: Electric current $I_{ref}(t) \simeq I_{av}(t)$ over time in the system* when applying constant voltage.

4.4 Test #3: Cascade Connection of ESC & PI Control

The same amount of whey protein and table salt is replicated (Test#2), but this time with the cascade ESC & PI Control, to compare if there is an improvement in fouling resistance growth.

The idea is to compare if there was an improvement in the reduction of fouling when applying the full control scheme (Test #3) versus applying only a constant voltage (Test#2).

Using the complete control scheme (Extremum Seeking Control & PI) proposed in figure 20 with setup of figure 24C:

Firs, the ED was cleaned by applying 10 $grams$ of caustic soda per liter of water and recirculating for half an hour. After cleaning, the hydraulic connection in Test#2 was used again. The results from figure 29 shows that the system's resistance $R_{av}(t)$ grows from 27.6 Ω to a maximum of 28.4 Ω, respectively, and the variation in resistance $\dot{R}_{av}(t)$ stabilizes at a value close to $0.005\ \Omega/seg$. To achieve optimization, the duty cycle DC_v saturates at its maximum of 96%. This implies a reference current I_{ref} that saturates at 1.38 A.

During the 800 $seconds$ of the test, the initial temperature in IBC1 was $17.3°C$ and increased to $19.7°C$. An important observation is made about the mathematical function representing $R_{av}(t)$. (3.22) in the simulation stage does not behave as expected because the plant available for testing has a small tank (IBC1) and does not have a cooler to maintain a constant or limited temperature as is the case with an industrial plant.

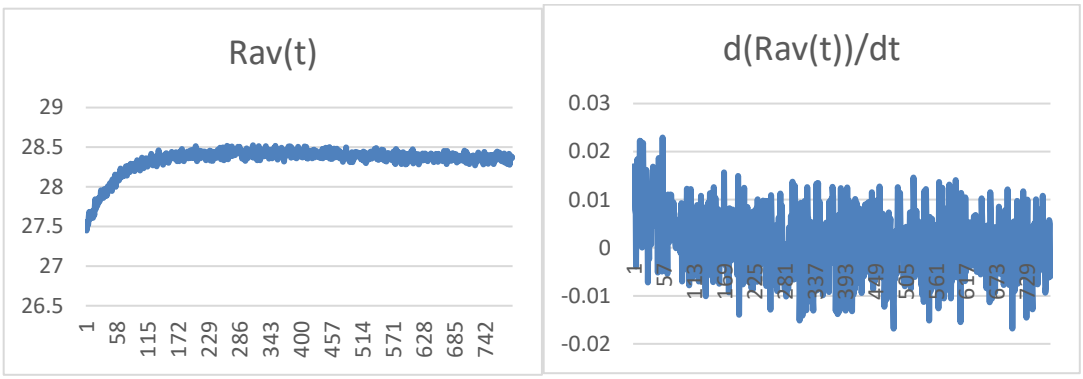

Figure 29: Left: Electrical resistance of the system $R_{av}(t)$ over time when applying voltage controlled by ESC & PI. Right: Variation in electrical resistance of the system $\dot{R_{av}}(t)$ over time when applying voltage controlled by ESC & PI.

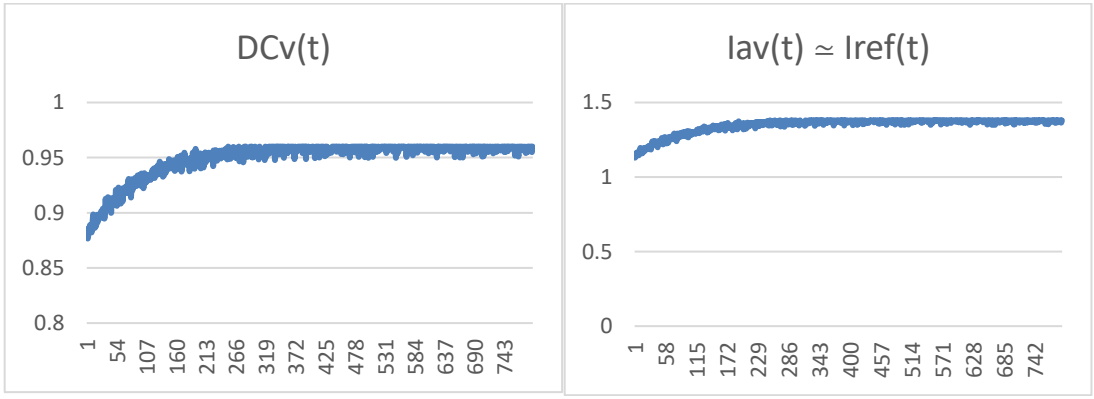

Figure 30: Left: Duty cycle DC_v of the input voltage over time in the system, controlled by ESC & PI. Right: Electric current I_{ref} over time in the system, controlled by ESC & PI.

The results obtained are encouraging for taking the ABS to a real industrial process. Currently, the **ABS** has been tested at the ARAUCO pulp plant in Valdivia, Chile, and has been able to operate successfully by using the pEDR method in the voltage applied to the ED of the industrial plant (which operates at 200Vdc with 20A), achieving improvements in delaying fouling.

These industrial-level results led to the initiation of a new project funded by CORFO and FONDECYT. This project aims, firstly, to make the ABS functional as a product in the industrial process, and secondly, to improve the control method explained in this manuscript. The goal is to implement an operating system on an industrial-grade computer and advance this control logic to an AI system that not only considers the electrical current and voltage sensors but also considers readings of flow rates, temperature, pressure, tank levels, conductivity and pH. As mentioned in Chapter 3, the mathematical model of the ED and the ESC control logic with cascaded PI control only monitor the electric current and the voltage applied to the ED.

If the AI is successfully implemented by the end of the project (year 2025), it is expected to not only yield positive results in improving the delay of fouling but also enhance the performance of desalination (purification) of the contaminated water from the KRAFT process.

It is expected that the use of ABS with ED at an industrial level will become the new standard for all pulp industries in the future, as it would be a method that consumes less energy, requires less maintenance (due to less fouling), and can purify (desalinate) contaminated water more quickly.

Chapter 5

Conclusions

This work constitutes industry-applied R&D, developed and validated in an industrial pilot plant at Arauco-Bioforest in collaboration with AC3E, under ANID Crea y Valida funding program and FONDECYT REGULAR 1231896.

The present work demonstrates that it is possible to obtain an electrical equivalent for a low-scale electrodialysis plant (power less than $40\ W$) a pEDR pulsed operation with an arithmetic extension, since the arithmetic extension depends on the number of IEMs (N) the errors of obtaining the components cannot be greater or less than 1 IEM of difference after the calibration method, since this would make the study meaningless and the individual contribution of each component that represents the electrochemical process.

On the other hand, empirically including an almost linear approximation of fouling through R_f and C_f is useful for the energy efficiency of the electrolyser over time, however this linear approximation is sufficient, but it does not represent the real fouling growth curve, since the real one presents three different growth zones that would not be possible to obtain with passive electrical elements. This electrical equivalence of the electrolyzing process has, after the calibration method, a maximum error of 9% in the resistance R_s and Z_{wo}, since they are more sensitive resistance magnitudes to the consideration of chemistry associated with ion dynamics and how the ED is assembled with its layers.

In general, obtaining the equivalent model of the electrochemical process of electrodialysis, both in its theoretical part (which includes R_M, C_{gs}, C_{dl}, R_s and Z_{wo}) and in its empirical part (R_f and C_f), can be generalized as the series connection of passive first-order low-pass filters (LPF-first order [35]). As the system becomes more complex, it is corrected by adding more LPF-first order filters.

To control purposes, the electrodialysis system is represented by an equivalent electrical model, approximated by a constant D for simplicity by combining it with a new function representing completely the fouling $R_f(t)$, it is sufficient to model the process and simulate a controller that reduces fouling growth.

In ED system simulated tests, it was observed that applying ESC & PI in cascade resulted in slower growth of average resistance compared to a constant voltage, indicating the effectiveness of the control scheme. The optimal performance is achieved when I_{ref} is $1.392A$, with DC_v at 92.6%, and a variation of average resistance result is $\dot{R}_{av} = 0.02\ \Omega/s$, the parameters of the ED is the same of the lab experiments of [22].

In the real pilot plant, the amplitude of fouling resistance $R_f(t)$ grows more slowly when using the pulsed Electrodialysis Reversal (pEDR) method (under a control method) compared to applying a constant voltage. In the $800\ second$ operation, applying ESC & PI instead of continuous voltage results in an improvement of $0.3\ \Omega$ less, despite the absence of temperature control in the system, this implies a more accelerated growth of the average system resistance, the improvement is evident when applying the developed controller.

Bibliography

[1] Urtenov, M Kh and Uzdenova, AM and Kovalenko, AV and Nikonenko, VV and Pismenskaya, ND and Vasil'Eva, VI and Sistat, P and Pourcelly, G, "Basic mathematical model of overlimiting transfer enhanced by electroconvection in flow-through electrodialysis membrane cells," *Journal of Membrane Science, Elsevier,* vol. 447, pp. 190--202, 2013.

[2] Strathmann, Heiner, "Electrodialysis, a mature technology with a multitude of new applications," *Desalination, Elsevier,* vol. 264, no. 3, pp. 268--288, 2010.

[3] Culcasi, Andrea and Gurreri, Luigi and Cipollina, Andrea and Tamburini, Alessandro and Micale, Giorgio, "A comprehensive multi-scale model for bipolar membrane electrodialysis (BMED)," *Chemical Engineering Journal, Elsevier,* vol. 437, 2022.

[4] Urtenov, Mahamet A-Kh and Kirillova, Evgeniya V and Seidova, Natalia M and Nikonenko, Victor V, "Decoupling of the Nernst- Planck and Poisson equations. application to a membrane system at overlimiting currents," *The Journal of Physical Chemistry B, ACS Publications,* vol. 111, no. 51, pp. 14208--14222, 2007.

[5] Choi, Eun-Young and Choi, Jae-Hwan and Moon, Seung-Hyeon, "An electrodialysis model for determination of the optimal current density," *Desalination, Elsevier,* vol. 153, no. 1-3, pp. 399--404, 2003.

[6] Patel, Sohum K and Qin, Mohan and Walker, W Shane and Elimelech, Menachem, "Energy efficiency of electro-driven brackish water desalination: Electrodialysis significantly outperforms membrane capacitive deionization," *Environmental science & technology, ACS Publications,* vol. 54, no. 6, pp. 3663--3677, 2020.

[7] Generous, Muhammad M and Qasem, Naef AA and Zubair, Syed M, "The significance of modeling electrodialysis desalination using multi-component saline water," *Desalination, Elsevier,* vol. 496, p. 114347, 2020.

[8] Mohammadi, Toraj and Moheb, Ahmad and Sadrzadeh, Mohtada and Razmi, Amir, "Modeling of metal ion removal from wastewater by electrodialysis," *Separation and Purification Technology, Elsevier,* vol. 41, no. 1, pp. 73--82, 2005.

[9] Galvanin, Federico and Marchesini, Raffaele and Barolo, Massimiliano and Bezzo, Fabrizio and Fidaleo, Marcello, "Optimal design of experiments for parameter identification in electrodialysis models," *Chemical engineering research and design, Elsevier,* vol. 105, pp. 107--119, 2016.

[10] Nikonenko, Victor V and Kozmai, Anton E, "Electrical equivalent circuit of an ion-exchange membrane system," *Electrochimica Acta, Elsevier,* vol. 56, no. 3, pp. 1262--1269, 2011.

[11] Sistat, Philippe and Kozmai, Anton and Pismenskaya, Natalia and Larchet, Christian and Pourcelly, Gerald and Nikonenko, Victor, "Low-frequency impedance of an ion-exchange membrane system," *Electrochimica Acta, Elsevier,* vol. 53, no. 22, pp. 6380--6390, 2008.

[12] Raka, Yash Dharmendra and Bock, Robert and Karoliussen, H{\aa}vard and Wilhelmsen, {\O}ivind and Stokke Burheim, Odne, "The influence of concentration and temperature on the membrane resistance of ion exchange membranes and the levelised cost of hydrogen from reverse electrodialysis with ammonium bicarbonatea," *Membranes, MDPI,* vol. 11, no. 2, p. 135, 2021.

[13] Mei, Ying and Tang, Chuyang Y, "Recent developments and future perspectives of reverse electrodialysis technology: A review," *Desalination, Elsevier,* vol. 425, pp. 156--174, 2018.

[14] Turek, M and Bandura, B, "Renewable energy by reverse electrodialysis," *Desalination,* vol. 205, no. 1-3, pp. 67--74, 2007.

[15] Bazinet, Laurent and Araya-Farias, Monica, "Effect of calcium and carbonate concentrations on cationic membrane fouling during electrodialysis," *Journal of colloid and interface science, Elsevier,* vol. 281, no. 1, pp. 188--196, 2005.

[16] Lee, Hong-Joo and Hong, Min-Kyoung and Han, Sang-Don and Cho, Seung-Hee and Moon, Seung-Hyeon, "Fouling of an anion exchange membrane in the electrodialysis desalination process in the presence of organic foulants," *Desalination, Elsevier,* vol. 238, no. 1-3, pp. 60--69, 2009.

[17] Lindstrand, Viktoria and Sundstrom, Goran and Jonsson, Ann-Sofi, "Fouling of electrodialysis membranes by organic substances," *Desalination, Elsevier,* vol. 128, no. 1, pp. 91--102, 2000.

[18] Vermaas, David A and Kunteng, Damnearn and Saakes, Michel and Nijmeijer, Kitty, "Fouling in reverse electrodialysis under natural conditions," *Water research, Elsevier,* vol. 47, no. 3, pp. 1289--1298, 2013.

[19] Hansima, MACK and Makehelwala, Madhubhashini and Jinadasa, KBSN and Wei, Yuansong and Nanayakkara, KGN and Herath, Ajith C and Weerasooriya, Rohan, "Fouling of ion exchange membranes used in the electrodialysis reversal advanced water treatment: A review," *Chemosphere, Elsevier,* vol. 263, p. 127951, 2021.

[20] Lee, Hong-Joo and Hong, Min-Kyoung and Han, Sang-Don and Shim, Joonmok and Moon, Seung-Hyeon, "Analysis of fouling potential in the electrodialysis process in the presence of an anionic surfactant foulant," *Journal of Membrane Science,* vol. 325, no. 2, pp. 719--726, 2008.

[21] Korngold, E and De Korosy, F and Rahav, R and Taboch, MF, "Fouling of anionselective membranes in electrodialysis," *Desalination, Elsevier,* vol. 8, no. 2, pp. 195--220, 1970.

[22] Gonzalez-Vogel, Alvaro and Rojas, Orlando J, "Exploiting electroconvective vortices in electrodialysis with high-frequency asymmetric bipolar pulses for desalination in overlimiting current regimes," *Desalination, Elsevier,* vol. 474, p. 114190, 2020.

[23] Marti-Calatayud, Manuel Cesar and Sancho-Cirer Poczatek, Mario and Perez-Herranz, Valentin, "Trade-off between operating time and energy consumption in pulsed electric field electrodialysis: A comprehensive simulation study," *Membranes, MDPI,* vol. 11, no. 1, p. 43, 2021.

[24] Uzdenova, Aminat M and Kovalenko, Anna V and Urtenov, Mahamet K and Nikonenko, Victor V, "Effect of electroconvection during pulsed electric field electrodialysis. Numerical experiments," *Electrochemistry Communications, Elsevier,* vol. 51, pp. 1--5, 2015.

[25] Junyong Hu, Shiming Xu, Xi Wu, Sixue Wang, Xuan Zhang, Shuaishuai Yang, Ruyu Xi, Debing Wu, Lin Xu, "Experimental investigation on the performance of series control multi-stage reverse electrodialysis," *Energy Conversion and Management,* vol. 204, p. 112284, 2020.

[26] Sahil R. Shah, Sandra L. Walter, Amos G. Winter, "Using feed-forward voltage-control to increase the ion removal rate during batch electrodialysis desalination of brackish water," *Desalination,* vol. 457, pp. 62-74, 2019.

[27] Ariyur, Kartik B and Krstic, Miroslav, Real-time optimization by extremum-seeking control, John Wiley & Sons, 2003.

[28] Gonzalez-Vogel, Alvaro and Rojas, Orlando J, "Asymmetric bipolar switch device for electrochemical processes," *AIP Advances, AIP Publishing,* vol. 9, no. 8, 2019.

[29] Goodwin, Graham C, Mario Salgado, Control System Desig, CONTROL SYSTEM DESIG, 2000.

[30] Donnan, Frederick George, "Theory of membrane equilibria and membrane potentials in the presence of non-dialysing electrolytes. A contribution to physical-chemical physiology," *Journal of Membrane Science,* vol. 100, no. 1, pp. 45--55, 1995.

[31] Le-Clech, Pierre and Chen, Vicki and Fane, Tony AG, "Fouling in membrane bioreactors used in wastewater treatment," *Journal of membrane science, Elsevier,* vol. 284, no. 1-2, pp. 17--53, 2006.

[32] Ixbalank Torres-Zúñiga, Fernando López-Caamal, Héctor Hernández-Escoto, Víctor Alcaraz-González, "Extremum seeking control and gradient estimation based on the Super-Twisting algorithm," *Journal of Process Control,* vol. 105, pp. 223-235, 2021.

[33] P. de Lamberterie, B. I. Godoy and J. S. Welsh, "Extremum seeking control applied to a model of the hall-héroult aluminium process," *UKACC International Conference on Control,* pp. 1-6, 2010.

[34] Erik Ayala-Bribiesca, Monica Araya-Farias, Gérald Pourcelly, Laurent Bazinet, "Effect of concentrate solution pH and mineral composition of a whey protein diluate solution on membrane fouling formation during conventional electrodialysis," *Journal of Membrane Science,* vol. 280, no. 1–2, pp. 790-801, 2006.

[35] Sedra, Adel S and Smith, Kenneth Carless, Microelectronic circuits, Holt, Rinehart and Winston, 1982.